A Future Techno-Economic Evaluation of an Offshore Wind-Hydrogen System with Battolyser Technology on the Dogger Bank

Thesis report

J.A. Wagener

Delft University of Technology

TU Delft

A Future Techno-Economic Evaluation of an Offshore Wind-Hydrogen System with Battolyser Technology on the Dogger Bank

by

J.A. Wagener

Student Name	Student Number
Name	Number
J.A. Wagener	4481089

TU Delft Supervisor:	Prof.Dr. A.J.M. van Wijk
Thesis committee:	Prof.Dr. F.M. Mulder
Thesis committee:	Dr. M.B. Zaayer
Institution:	Delft University of Technology
Place:	Faculty of EEMCS, Delft

TU Delft

Preface

In this work, I summarize my knowledge gained from my master's degree in Sustainable Energy Technology over the past two years. I look back on an eventful year with many ups and downs. I was able to gain a lot of knowledge about new technologies and I took my academic skills to the next level. I can say that I am proud of the work I have accomplished, but of course, I did not do this alone.

Therefore, I would like to thank Siddharth Kalra for his meticulous feedback, which pushed me to take my thesis to the next level. Additionally, I am grateful to my supervisor, Ad van Wijk, for his invaluable guidance and insights as a hydrogen expert. Furthermore, I want to express my thanks to Fokko Mulder and Michiel Zaayer for their support and expertise as committee members.

My friends made my academic journey all the more enjoyable, and I am grateful for their companionship. Finally, I owe a debt of gratitude to my family for their unwavering support and my girlfriend for her boundless patience throughout my studies.

J.A. Wagener
Delft, March 2023

Abstract

Dutch offshore wind farms are primarily located near the coast and connected to the grid, but as offshore wind farms continue to expand and occupy more space, developers are turning to deeper waters. However, installing traditional monopile or jacket structures in these deeper waters can be expensive. One potential solution is the Dogger Bank, a shallow sand bank located 275 km from the Dutch coast, which allows for inexpensive wind turbine installation and high capacity factors. For far offshore locations like the Dogger Bank, electricity transport can be costly, making hydrogen transport via the existing gas infrastructure a more efficient solution. This could enable hydrogen production far offshore and its use in the decarbonisation of hard-to-abate sectors.

This study focuses on the development of a stand-alone offshore hydrogen production system, incorporating battolyser technology, on the Dogger Bank. The battolyser, which combines a Ni-Fe battery and an alkaline electrolyser, is able to store energy and produce hydrogen efficiently and flexibly. However, as the battolyser is not yet commercially available, the proposed systems are analysed for the years 2030 and 2050. The study examines three system configurations: an electrolyser-battolyser, battolyser-only, and electrolyser-battery configuration. For the electrolysers, alkaline and PEM electrolysis is considered. For the battery a vanadium redox flow battery (VRFB).

To ensure autonomous operation, the battolyser serves as a backup power source for supplying the system's auxiliary energy demand. This demand is used to determine the system's sizing, and a MATLAB/Simulink model is developed to calculate the hydrogen production based on future estimates of technical parameters. The hourly wind data from offshore platforms near the Dogger Bank is used as input for the model. To project future capital expenditures (CAPEX) for the model components, a learning curve method is employed, which assumes a specific cost reduction rate with every doubling of cumulative installed capacity.

This study demonstrates the feasibility of an offshore wind-hydrogen system with battolyser technology, both technically and economically. Battolyser CAPEX are used as an input variable to estimate a range of possible levelized cost of hydrogen (LCOH) values for different systems. The study findings indicate that LCOH values of less than 1.55 €/kg could be achieved by 2030, and by 2050, these values could drop to less than 1.18 €/kg.

Contents

Nomenclature

Abbreviations

Abbreviation	Definition
AE	Alkaline electrolysis
AEB	AE-battolyser
AEV	AE-VRFB
AF	Annuity factor
B	Battolyser
BoP	Balance of Plant
CAPEX	Capital Expenditures
DGB	Dogger Bank
EEZ	Exclusive Economic Zones
HHV	Higher Heating Value
HVAC	High Voltage Alternating Current
HVDC	High Voltage Direct Current
KNMI	Koninklijk Nederlands Meteorologisch Instituut
LHV	Lower Heating Value
LCOH	Levelised Cost Of Hydrogen
NSWPH	North Sea Wind Power Hub
OPEX	Operational expenditures
PEM	Polymer Electrolyte Membrane
PEMB	PEM-battolyser
PEMV	PEM-VRFB
PMSG	Permanent Magnet Synchronous Generator
RO	Reverse Osmosis
SWRO	Seawater Reverse Osmosis
VRFB	Vanadium Redox Flow Battery
WACC	Weighted Average Cost of Capital

Symbols

Symbol	Definition	Unit
AF	Annuity factor	[-]
CAP	Installed capacity	[GW]
$CAPEX$	Capital expenditures	[€/kW]
C_P	Power coefficient	[-]
Δt	Time period of consecutive hours	[h]
E	Energy	[kWh]
F	Charge utilisation factor	[-]
h	Height	[m]

Symbol	Definition	Unit
I	Current	[A]
$LCOH$	Levelised Cost of Hydrogen	[€/kg]
LT	Lifetime	[h]
$\dot{m}_{H_2}$	Hydrogen production rate	[kg/h]
$OPEX$	Operational expenditures	[€/kW]
p	Pressure	[bar]
P	Power	[kW]
r	Discount rate	[%]
R	Radius	[m]
SOC	State of Charge	[-]
T	Temperature	[$^{\circ}$C]
U	Wind speed	[m/s]
$WACC$	Weighted Average Cost of Capital	[%]
z_0	Roughness length	[m]
α	Power coefficient	[-]
η	Efficiency	[%]
ρ	Air density	[kg/m^3]
θ	Load	[%]

List of Figures

List of Tables

1

Introduction

Context

To reach the EU's ambitious future energy and climate targets, the European Commission (EC) has proposed a strategy aiming at 300 GW of offshore wind capacity by 2050 [1]. However, it is unlikely that the future energy system's requirements will be met only by electricity production. Therefore, offshore hydrogen production can play a key role in the EU's future energy system, especially in hard-to-abate sectors, such as heavy industry and long-haul transport [2].

An interesting location for an offshore wind-hydrogen system is the Dogger Bank. The Dogger Bank is a large sandbank in the North Sea, 275 km from the Dutch coast. For far offshore locations like this, transporting energy in the form of hydrogen is significantly cheaper than energy in the form of electricity [3]. Furthermore, the Dogger Bank is specifically attractive because of its shallow waters, high wind speeds and existing gas infrastructure [4]–[6] These characteristics are essential drivers for cheap offshore hydrogen production.

An off-grid system must be designed for far offshore installations dedicated to hydrogen production. In this study, a system design is introduced, including battolyser technology. The battolyser is a novel promising technology that enhances the case for a grid-independent, offshore wind-hydrogen system. A battolyser can be described as a combination between a Ni-Fe battery and an alkaline electrolyser. Hydrogen is increasingly produced upon charging the battolyser, reaching a maximum hydrogen production rate at full charge [7]. The battolyser can efficiently switch between hydrogen production and battery discharge for many subsequent cycles [7]. The functionalities of the battolyser enable efficient exploitation of far offshore regions. The battolyser makes grid independence possible by supplying the system's power demand during periods of low wind. During surpluses of wind energy, the battolyser produces hydrogen, resulting in a higher energy utilisation factor than other battery systems.

Only one identified techno-economic analysis in literature investigates the use of battolyser technology in offshore wind-hydrogen systems. Jenkins et al. (2022) conducted this analysis on a grid-connected offshore wind-battolyser system, which focuses on the levelised cost of energy, based on the combined electricity and hydrogen production and sales [8]. However, an assessment has yet to be made for an autonomous wind-hydrogen system that incorporates battolyser technology and focuses solely on hydrogen production.

The full technical and economic potential of offshore hydrogen production in the North Sea can be enabled by implementing battolyser technology. This would be essential to reaching the EU's future energy and climate targets.

Objective and scope

The purpose of this study is to develop and evaluate a self-contained offshore wind-hydrogen system with battolyser technology located on the Dogger Bank. This offshore system must be durable and robust enough to operate in a remote location. Since the battolyser technology is still emerging, the system configuration will be designed for the years 2030 and 2050. This study does not consider the specific end-users of the hydrogen produced, and hence hydrogen compression and transport will not be included in the analysis. To effectively evaluate the battolyser's performance, a battery-inclusive system will also be evaluated. The research question that summarizes the objectives of this study is as follows:

Is it technically and economically feasible to design a stand-alone offshore wind-hydrogen system, that incorporates battolyser technology, located on the Dogger Bank, in the years 2030 and 2050?

To answer the research question, the following sub questions are answered successively:

- What system configurations are possible to enable autonomous operation of an offshore wind-hydrogen system?
- What are the future cost projections of the individual system components?
- How do the different offshore wind-hydrogen system designs compare with respect to their performance and levelised cost of hydrogen?
- What is the acceptable cost range for the battolyser technology in an offshore wind-hydrogen system that would justify its implementation?
- What are the key parameters that have a significant impact on the analysis results for offshore wind-hydrogen system designs, and how sensitive are the results to changes in these parameters?

Report outline

The structure of the report is as follows:

Section 2 begins by evaluating the suitability of the Dogger Bank location for an offshore wind-hydrogen system, followed by an overview of the theory underlying the different components of the system. Lastly, the feasibility of in- or at-the-turbine electrolysis is examined.

Section 3 outlines the methodology used in the study, starting with an explanation of the modelling process and possible system configurations. The criteria used to size the system are described, and the implementation of individual components in the model is explained. Finally, future costs of the system's components are calculated.

Section 4 presents the results of the study, followed by a discussion where the results are interpreted and where the limitations of this study are explained.

Finally, the conclusion summarizes the findings of the study and provides recommendations for future research on the subject.

2

Literature review

This chapter assesses the suitability of the Dogger Bank location for a wind-hydrogen system. Section 2.1 provides a description of the Dogger Bank and discusses its protected status and physical characteristics. It is explained how these characteristics make it favorable for the assessed system. Section 2.2.2 explains the theory and operational characteristics of the system components, while Section 2.3 investigates the structural feasibility of the system.

2.1.Dogger Bank location analysis

The Dogger Bank, a sandbank situated in the North Sea and spanning across the waters of the UK, Germany, Denmark, and the Netherlands, is an attractive location for offshore wind farms due to its water depth, wind speeds, and ample space [5][6]. The Dogger Bank is divided by the Exclusive Economic Zones (EEZs) of these countries, which grant them rights to exploit and explore energy production from various sources, including wind and water [9]. With an area of almost 22,000 km^2, the Dutch EEZ covers approximately 4,800 km^2 of the Dogger Bank, and the distance from Den Helder, Netherlands to the sandbank is approximately 275 km.

To ensure compliance with the Natura 2000 program, the Dogger Bank, a protected area, requires a thorough evaluation before assigning wind energy production areas. While some areas have already been designated as wind energy production areas in the UK, the Netherlands has yet to do so. However, this study assumes that the Netherlands will allocate parts of the Dogger Bank as wind energy production areas from 2030 onwards, based on increasing space constraints near the shore, a growing demand for green energy, and technological advancements that allow the coexistence of wind farms, flora, fauna, and fisheries. By 2026, all three phases of the Dogger Bank wind farms (A, B, and C) will be operational, with a total installed capacity of 3.6 GW [10].

In 2016, Tennet took the initiative to form a consortium that investigates the possibilities of producing wind energy in the North Sea. The consortium introduced the North Sea Wind Power Hub (NSWPH), a large-scale, far offshore facility that utilizes the 'Hub-and-Spoke' concept to connect wind farms to centrally located hubs. These hubs are then linked to the surrounding North Sea countries. Additionally, the potential use of power-to-x, a process that converts electricity to another energy carrier, is being considered. The Dogger Bank is a technically and economically promising location, but obtaining agreement with environmental stakeholders remains a challenge. Despite the proven feasibility of installing wind farms in the Dogger Bank, this paper will examine the site's characteristics and conditions in more detail.

According to a long-term (1958-2012) simulation of the average wind speed at a height of 100 m shown in Figure 2.1, the wind speed increases when moving further offshore and to the northern region of the North Sea. The simulation demonstrates that the average wind speed at the Dogger Bank (DGB) is 10.1 m/s, which is the high compared to other existing

and potential wind farm locations in the North Sea. The Dogger Bank's comparatively high wind speed compared to other locations in the North Sea makes it a desirable site for installing offshore wind farms [5].

The wind speeds in Figure 2.1 are used to show the potential of the Dogger Bank compared to other wind farms. For the model, the wind speed data is extracted from KNMI data sets [11], and will be elaborated on in Section 3.3

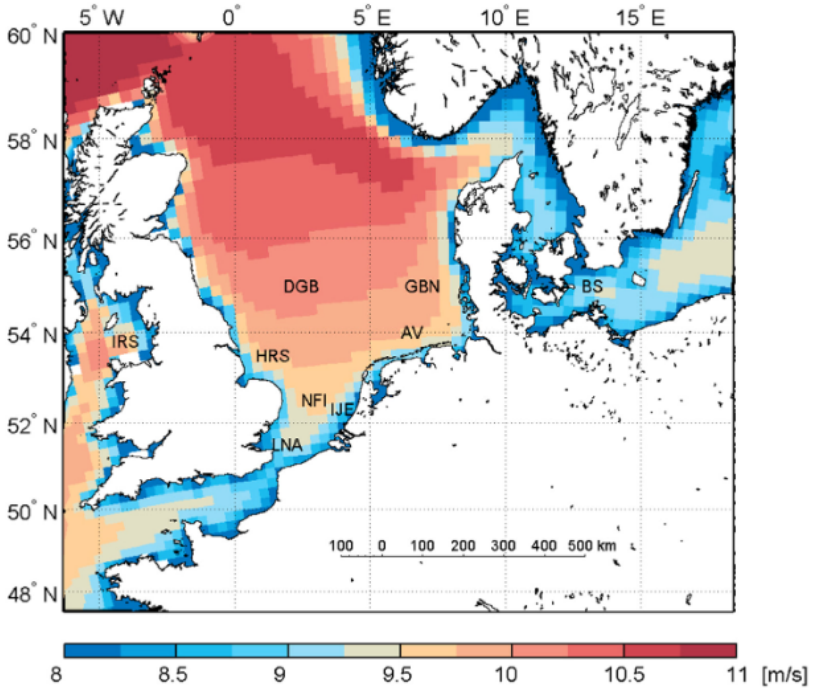

Figure 2.1: Long term (1958-2012) average wind speeds at the North Sea at a height of 100 metres. The abbreviations related to the locations of the wind farms. Dogger Bank is abbreviated as "DGB" [5]

For offshore wind installations, the water depth is an important cost factor. As wind turbines are placed further and further offshore, the increasing water depths yield higher production and installation costs for monopile foundations, because of the increasing length and weight. One of the main advantages of the Dogger Bank is the relatively shallow water. Figure 2.2 shows the bathymetry at the location of the Dogger Bank. The depth at the Dogger Bank varies between -15 m and -40 m [12]. This study focuses on the northern Dutch EEZ of the Dogger Bank, where the water depth is approximately between -20 m and -40 m. In this range, the total available area for the installation of wind farms in the Dutch EEZ is 4793 km^2, which corresponds to a potential offshore wind energy capacity of 24 GW [6].

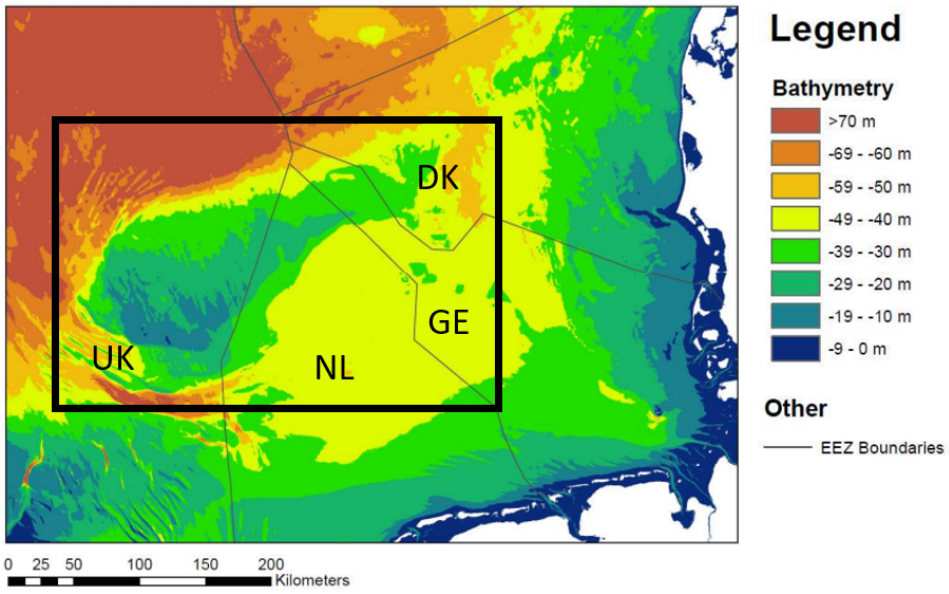

Figure 2.2: Bathymetric map of the North Sea, where the Dogger Bank is outlined by the black frame. Within the black frame the Exclusive Economic Zone (EEZ) boundaries for the UK, the Netherlands (NL), Germany (GE) and Denmark (DK) are displayed [12]

It seems like there is a lot of space in the Dutch North Sea close to shore, but a large part of this space is already occupied by (future) wind farms, oil- and gas platforms, pipelines and power cables. Furthermore, the infrastructure consists of areas designated as shipping routes, fishing areas, nature reserves and Defense training areas. The Dogger Bank, however, is still relatively undeveloped in terms of human activity. Being able to accommodate far offshore wind turbines in terms of space is an advantage that becomes more important as close to shore location become scarce. The only structures that are currently present, are some gas production platforms operated by Chevron. The use case for the hydrogen produced by the system is irrelevant for this study, as the focus lies on analysing the implementation of battolyser technology. However, the choice of this location makes it possible to easily connect with the existing gas network, the surrounding gas platforms and possibly with future North Sea energy hubs.

The specific characteristics of the Dogger Bank suggest that it has the potential to support wind energy generation. Since the distance between the Dogger Bank and the shore is around 275 km, it is more cost-effective to transport wind energy in the form of hydrogen rather than electricity. The transmission of electricity via HVAC cables becomes uneconomical for distances greater than 100 km due to high energy losses. Transmission with HVDC cables can reduce these losses, but it requires expensive offshore power conversion [13]. Adapting the existing gas infrastructure to transport hydrogen would cost only 5-10% of the price of building a new pipeline [3]. Comparing the BritNed cable and the BBL gas pipeline shows that hydrogen transport via an existing gas infrastructure is significantly more efficient than transporting electricity via new cables [3].

Table 2.1: Comparison between the BritNed cable and the BBL gas pipeline [3]

	BritNed cable	**BBL gas pipeline**
Capacity	1 GW	15 GW
Length	276 km	225 km
Construction cost	€500 million	€500 million
Annual volume	8 TWh	120 TWh

2.2.Model components

2.2.1.Wind turbine

On the Dogger Bank within the UK EEZ, there are currently four offshore wind projects under development, namely Dogger Bank A, B, and C, as well as the Sofia Offshore Wind Farm. Collectively, these projects will generate 5GW of offshore wind power, utilizing both General Electric's 'Haliade-X 14MW' turbines and Siemens Gamesa's 'SG 14-222DD' (14MW) turbines [14], [15]. Detailed information on the tower and foundation dimensions of both turbines is not available. Therefore, this study adopts the 'IEA Wind 15-Megawatt Offshore Reference Turbine' [16] as a reference for the model, given its open design and publicly available design parameters. This reference turbine is designed for a 15 MW offshore wind turbine.

Technology description

The reference turbine is a direct-drive wind turbine. Direct-drive means that the hub is directly connected to the generator without the use of a gearbox. Direct drives are interesting for offshore wind turbines as the absence of a gearbox implies less downtime. Therefore, lower maintenance costs offers higher reliability. Because the hub is directly connected to the generator the rotational speed is low. To produce the a certain amount of power at low rotational speed the applied torque has to be larger and, consequently, the size of the generator increases. The generator is a Permanent Magnet Synchronous Generator (PMSG). The PMSG consists of a rotor equipped with permanent magnets and a stator with coils. Mechanical rotational energy is converted to electrical energy by the rotor inducing an electrical current in the coils in the stator.

For water depths up to 40m, monopiles are the preferred foundation in terms of cost, transportability and ease of installation and deconstruction. Jacket structures are mostly used in water depths between 40m-60m. Floating structures are typically more economically viable compared to bottom-fixed foundations in water depths of 60 metres and deeper. The reference turbine is supported by a 75m monopile of which, of which 45m is embedded in the sea bottom. The hub height is 150m and the rotor blades span a diameter of 240m. These physical properties allows the wind turbine to operate in 30m deep waters keeping a 30m water surface clearance [16]. According to the bathymetry discussed in Section 2.1, the reference turbine fits the location and no further assumptions regarding monopile length have to be made. The transition piece connects the wind turbine to the monopile foundation and accommodates various functionalities, such as a boat landing, cable connections, and corrosion protection for the foundation. In the case of this research, the transition piece may be used for placing the hydrogen production system as well. Transition pieces vary in size and shape per project.

Auxiliary power demand

Offshore wind turbines require uninterrupted operation of their electrical systems, such as

mechanical system controllers, safety systems, lighting, and nacelle climate regulation (heating and dehumidification), even during low or no wind conditions [17], [18]. As a result, small batteries or ultracapacitors are often integrated into large wind turbines to supply power to these systems. Normally, when these sources are depleted, electricity is drawn from the grid, but since the system in this study is not connected to the grid, a battolyser or battery will supply power to the 15MW reference turbine. The auxiliary power demand of a 6MW wind turbine made by REpower is 42kW, and the power capacity of the reference turbine in this study is 2.5 times larger than that of the REpower wind turbine [19]. Hence, the power demand for the 15MW reference turbine is estimated to be 100kW.

2.2.2.Electrolysers

Electrolysis is a chemical reaction where water is split into hydrogen and oxygen under an applied voltage. The two half-reactions take place at the positive (anode) and negative (cathode) electrode, where the hydrogen is produced at the cathode and oxygen at the anode. As these half-reactions take place, the charge is kept in equilibrium by the transport of ions through a conductive substance called electrolyte. A membrane separates the electrodes to prevent the produced gasses from mixing.

In this research two key electrolyser technologies are compared and modelled: Alkaline Electrolysis (AE) and Polymer Electrolyte Membrane (PEM) electrolysis. AE is the most mature technology and is widely adopted for the production of hydrogen. PEM electrolysis is an emerging technology that is rapidly increasing in popularity and market share [20].

Alkaline electrolysis

Since the 1920s, alkaline electrolysers are used for large-scale industrial applications [21]. In Figure 2.3 a schematic diagram of the alkaline electrolysis process is presented, together with the half-reactions at the anode and cathode. The electrodes are mostly made out of nickel as nickel is highly cost effective and stable in potassium hydroxide (KOH) solutions [22]. The electrodes are submerged in a KOH solution that allows for the conductivity of hydroxide (OH^-). The diaphragm separates the anode and the cathode and serves as a porous membrane. The membrane only allows OH^- transport and makes sure the product gasses O_2 and H_2 stay separated in the electrolyte.

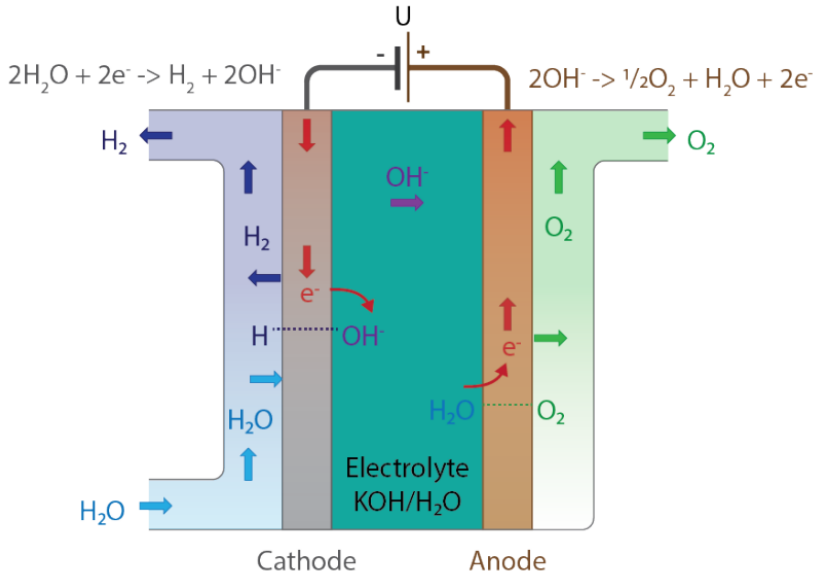

Figure 2.3: Conceptual representation of an alkaline electrolyser [22]

Compared to PEM technology, alkaline electrolysers have the lowest overall system costs because of the use of low cost material like nickel electrodes and the maturity of the technology. Also, the exchangeability of the electrolyte and stability of nickel in the KOH solution contribute to the longevity of the system. The main disadvantages of alkaline electrolysers are their limited operating range and relatively low operating current densities. The operating range is limited at the lower boundary, which is caused by increasing gas impurities at decreasing current densities. The intermixing of produced gasses is prevented by increasing the thickness of the diaphragm. However, increasing the diaphragm thickness increases the ohmic resistances, which reduces the current density at an applied voltage. In new advanced designs, thinner diaphragms and zero-gap configurations are applied to increase the current density. It is questionable however, if these improvements come at the cost of the stability and robustness present alkaline electrolysers have to offer [23]. The relatively low operating current density causes alkaline electrolysers to be large and heavy in comparison to other technologies. This might be crucial in applications where space and weight limitations apply.

PEM electrolysis

PEM electrolysers do not use an electrolyte fluid, but a solid polymer electrolyte membrane like Nafion is used. Nafion has a high density of bound HSO_3. As it takes up some of the H_2O it allows for the H^+ ions to be conducted through the polymer upon applying a voltage to the electrodes. PEM electrolysers require noble metal catalysts. For the anode and cathode, typically iridium oxide and platinum are used, respectively [24].

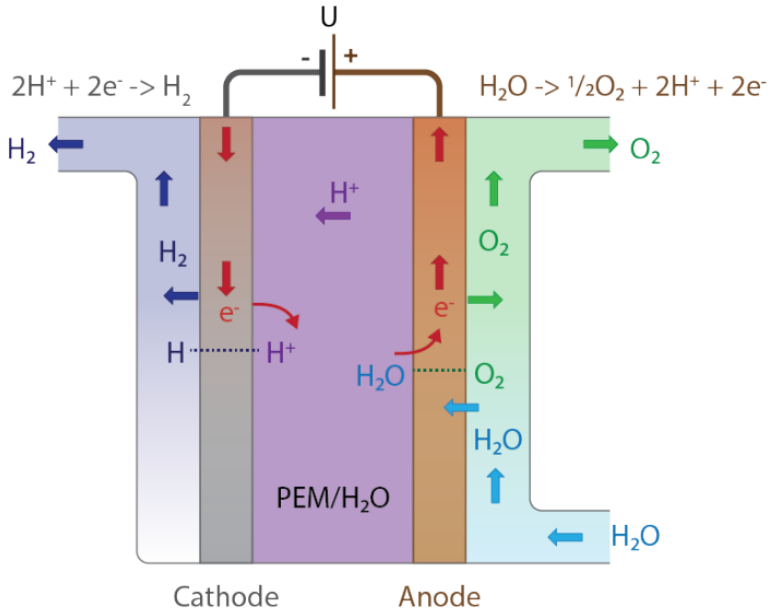

Figure 2.4: Conceptual representation of a PEM electrolyser [22]

PEM electrolysers have several advantages. Firstly, with PEM electrolysis the concerns for corrosion are less as the acid is contained in the PEM-material. Secondly, PEM is a solid, so the electrolyser can operate with a very thin membrane while keeping the gases separated. The thin membrane enables lower internal resistance and higher possible current densities. Finally, PEM electrolysers are better capable of handling a short term variable power supply. However, this forms no problem for wind turbines. Due to the inertia of rotor mass there are no really short term variations in power supply. The disadvantages of PEM electrolysis mainly relate to high system costs, which results from the use of noble metals and Nafion. Also, PEM electrolysers currently have shorter lifetimes than alkaline electrolysers, which translates to higher costs as well [24].

Electrolyser efficiency

The efficiency of an electrolyser is a crucial aspect when evaluating the performance of a system. Its efficiency is influenced by both its internal system boundaries and the larger system in which it operates. This paper will analyze different definitions of energy efficiency, beginning at the stack level.

The efficiency of a stack, also known as the DC efficiency, can be expressed as the multiplication of the Faraday efficiency and the voltage efficiency. The Faraday efficiency refers to the effectiveness of charge transfer within the system, while the voltage efficiency refers to the ratio of the thermoneutral voltage (1.48V) and the cell voltage, accounting for losses from overpotentials and ohmic losses. The operating point is another critical factor that influences DC efficiency. As the current density increases, the amount of hydrogen produced also rises. However, higher current densities can cause a corresponding increase in cell voltage, leading to decreased voltage efficiency [25].

Moreover, the DC efficiency can be measured using either the Higher Heating Value (HHV) or the Lower Heating Value (LHV). HHV considers the heat of vaporization of water in the combustion products, whereas LHV does not. In this study, HHV is adopted as the standard since it assumes that maximum heat capture is achievable in industrial systems [26].

Defining the DC efficiency is relatively straightforward. On the other hand, the overall efficiency of an electrolyser system can vary depending on the system's configuration and application. Figure 2.5 provides a schematic illustration of the system efficiency, voltage efficiency, and Faraday efficiency. In partial load operation, the voltage efficiency tends to increase, while the Faraday efficiency decreases.

The present study involves systems that are connected directly to the DC-link of wind turbines, eliminating the need for AC rectification. Moreover, hydrogen production is evaluated directly at the output of the electrolyser. This means that hydrogen transportation and mechanical hydrogen compression are outside the scope of this study. Due to this unique system configuration and the direct analysis of hydrogen production at the electrolyser output, the system efficiency is assumed to be equivalent to the DC efficiency at the stack level. Section 3.4.2 will provide further details on the implementation of partial load efficiency of PEM and AE in the model.

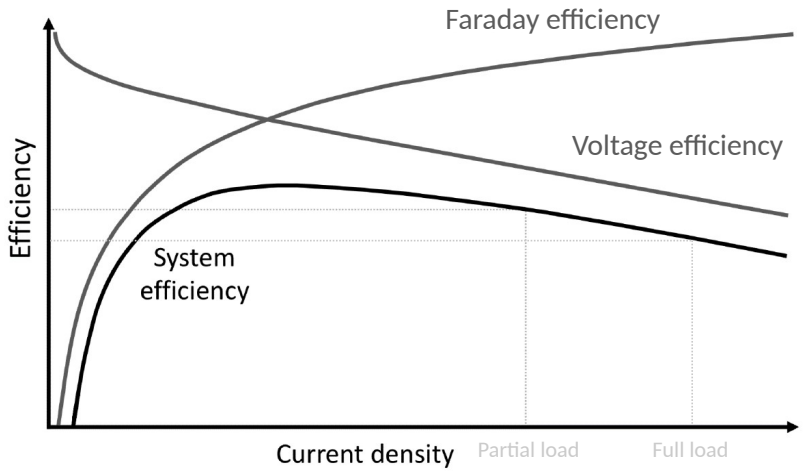

Figure 2.5: Schematically presented system efficiency, voltage efficiency and Faraday efficiency [25]

Auxiliary power demand

The electrolyser can operate in three modes depending on the power input. If the power input is above the minimum load requirement, the electrolyser is in operating mode and produces hydrogen based on the power input. When the power input falls below the minimum load requirement, the electrolyser switches to standby mode, which can be either hot or cold. In cold standby mode, the system is not producing hydrogen, and the power consumed is less than 1% of the nominal power capacity of the electrolyser, primarily related to the power usage of the electrical safety infrastructure [27]. Since the power consumption in cold standby is negligible, switching to cold standby mode is considered equivalent to shutting down the electrolyser. According to literature, the maximum acceptable number of shutdowns throughout the electrolyser's lifespan can range from several thousand to 5000 [28], [29]. In hot standby mode, the system is also not producing hydrogen, but power is consumed to maintain the electrolyser system at operating pressure and temperature, ensuring a fast response to the wind turbine output and ramping up hydrogen production within seconds. The power consumption in hot standby mode is equivalent to 2% of the nominal power capacity of the electrolyser [27].

2.2.3.Battolyser

The previous section introduced the concept of the battolyser and its operating context. The subsequent sections will focus on the technical aspects of the battolyser. Specifically, the technology behind the battolyser will be explained, followed by a discussion of its behaviour and performance.

Technology description

Battolyser technology integrates the functionality of a Ni-Fe battery and alkaline electrolysis in a single system. In Figure 2.6, a schematic diagram of the battolyser is presented together with the half-reactions at the electrodes.

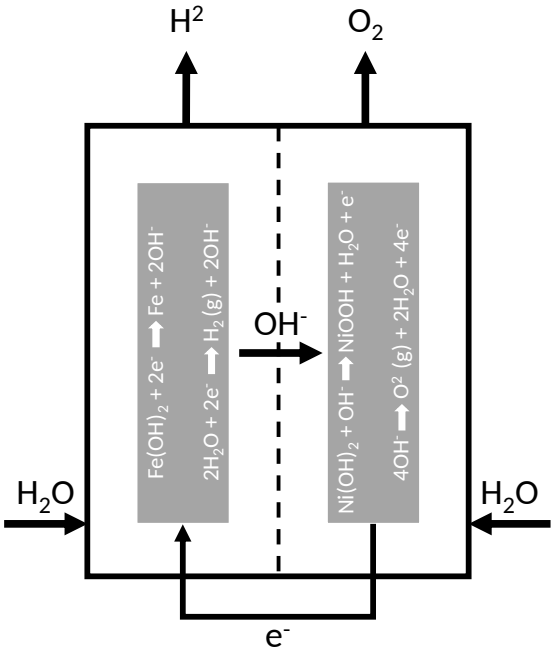

Figure 2.6: Schematic representation of the battolyser [30]

The battolyser comprises a positive Ni(OH)2 electrode and a negative Fe(OH)2 electrode, which are immersed in a KOH electrolyte. These electrodes are separated by a ceramic polymer composite diaphragm that allows for the flow of OH- ions between them. When the battolyser is charged, protons and OH- ions are released at the positive and negative electrodes, respectively, leading to the production of hydrogen via an alkaline electrolysis process. The rate of hydrogen production increases as the battery state-of-charge (SOC) increases. This is because more Fe and NiOOH are available, which act as catalysts for hydrogen and oxygen evolution, respectively. The maximum rate of hydrogen production is reached when the battery is overcharged and reaches its nominal capacity. According to laboratory tests on single cells conducted by Mulder et al. (2017), the maximum saturation capacity of the battery is 1.45 times greater than its nominal capacity. In the past, it was not possible to fully utilize the electrode material due to the significant amount of hydrogen and oxygen produced when the battery reached its nominal capacity, leading to historically low Ni-Fe efficiencies [30].

Battolyser efficiency

The battolyser energy efficiency is the sum of its battery and electrolysis efficiency. The

battery's efficiency is evaluated using the round-trip efficiency, while the electrolysis efficiency follows the same principles explained in Section 2.2.2. Empirical studies have demonstrated that the total Faradaic efficiency of the battolyser is 100±0.5% [30]. However, the current in a battolyser is split between its battery and electrolysis components, with the utilization factors of each depending on the state of charge of the battery. This state of charge is determined by Equations 2.1 and 2.2 [30].

$$F_{b,el} = \frac{I_{b,el}}{I_b} = 1 - \left(\frac{4 \exp\left(-2 \cdot SOC\right)}{\left(1 + \exp\left(-2 \cdot SOC\right)\right)^2} \right) \tag{2.1}$$

and

$$F_{b,b} = \frac{I_{b,b}}{I_b} = \left(\frac{4 \exp\left(-2 \cdot SOC\right)}{\left(1 + \exp\left(-2 \cdot SOC\right)\right)^2} \right) \tag{2.2}$$

where $I_{b,el}$ is the current dedicated to electrolysis, $I_{b,b}$ is the current dedicated to the battery and I_b is the total current inserted in the battolyser.

Figure 2.7 displays the characteristic curves. The maximum battery saturation is attained at the intersection of the two curves. Beyond this point, the majority of the current is allocated for electrolysis. Nevertheless, the battery charge curve suggests that a fraction of the current is still assigned to the battery after reaching the maximum saturation point. This fraction is linked to battery losses, such as heat production.

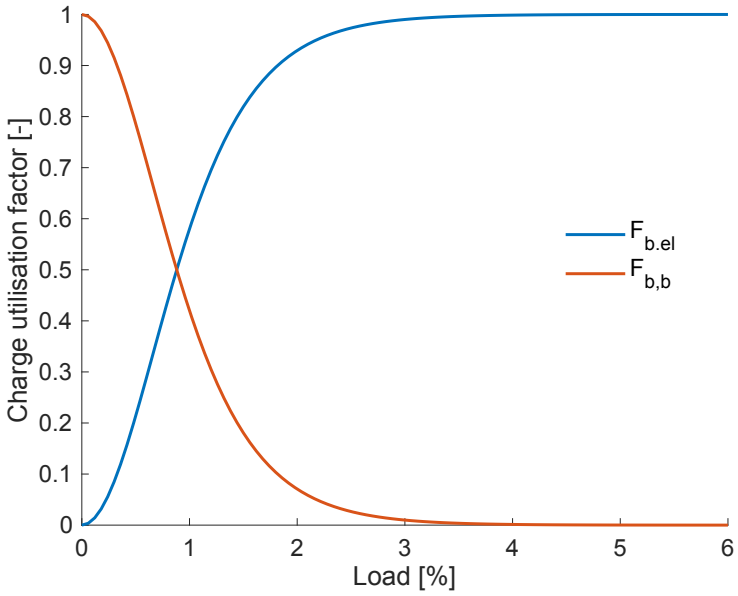

Figure 2.7: Charge utilisation curves for battery charge and electrolysis as a function of the SOC of the battery portion [7].

The characteristics of the voltage efficiency curve of the battolyser are comparable to those of a dedicated alkaline electrolyser [30]. Consequently, the voltage efficiency curve of the alkaline electrolyser is adopted for efficiency calculations of the battolyser. The partial load efficiency of hydrogen production by the battolyser is computed by multiplying the voltage efficiency with

the charge utilisation factor ($F_{b,el}$) at a particular load and state of charge (SOC). The model's implementation of partial load efficiency is elaborated in Section 3.4.3.

2.2.2.

2.2.4.Vanadium redox flow battery

Flow batteries are electrochemical energy storage systems that use two electroactive materials separated by a membrane to store energy. The two electroactive materials, usually liquids, are circulated through separate tanks and flow into a stack when energy is needed. Flow batteries are different from traditional batteries as they can provide continuous and flexible power over an extended period. In addition, the capacity of a flow battery can be easily scaled up by increasing the size of the storage tanks.

A Vanadium Redox Flow Battery (VRFB) is a flow battery that uses vanadium ions in different oxidation states to store and release energy. VRFBs are known for their long cycle life, high efficiency, and easy scalability [31].

A VRFB consists of two electrolyte solutions containing vanadium ions in different oxidation states (V2+/V3+ and V4+/V5+). The two solutions are stored in separate tanks and pumped through the electrolyte chamber of the battery, which contains a proton exchange membrane. The membrane keeps the two electrolytes separate, allowing protons to pass through while preventing mixing of the two solutions. A schematic of a VRFB is presented in Figure 2.8

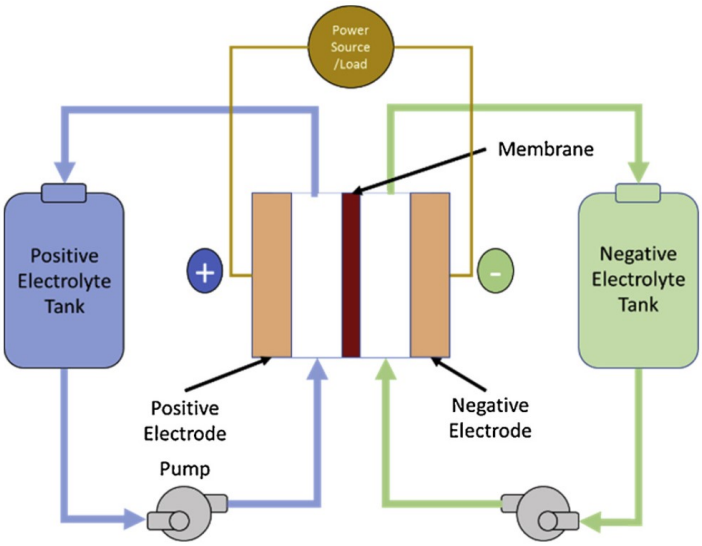

Figure 2.8: Schematic representation of a vanadium redox flow battery [32]

When the battery is charged, electrons are extracted from the V2+/V3+ solution and fed into the V4+/V5+ solution, causing the oxidation state of the vanadium ions to change. The charged electrolyte is stored in a separate tank until energy is needed. When the battery is discharged, the charged electrolyte is pumped back through its electrolyte chamber, which releases electrons that flow through an external circuit, generating electricity. This processes of charging and discharging are depicted in Figure A.1 and A.2.

2.2.5.Desalination unit

Research shows that desalination through reverse osmosis (RO) can be considered as the most suitable technology for the system design in this study. This is because RO has the lowest unit cost and consumes the least energy among the various desalination technologies, while providing sufficient water quality [33]. Just like the other system components, the desalination unit would be placed in- or at the turbine.

Despite the necessity of including a desalination unit in the system, the contribution to the energy consumption and total cost of the system is negligible. In a study by Kahn et al. (2021) the energy and cost contribution of seawater reverse osmosis (SWRO) analysed for a PEM-SWRO system [34]. It was found that the SWRO unit adds <0.1$ per kg H_2. An energy and cost breakdown is shown in Figure 2.9.

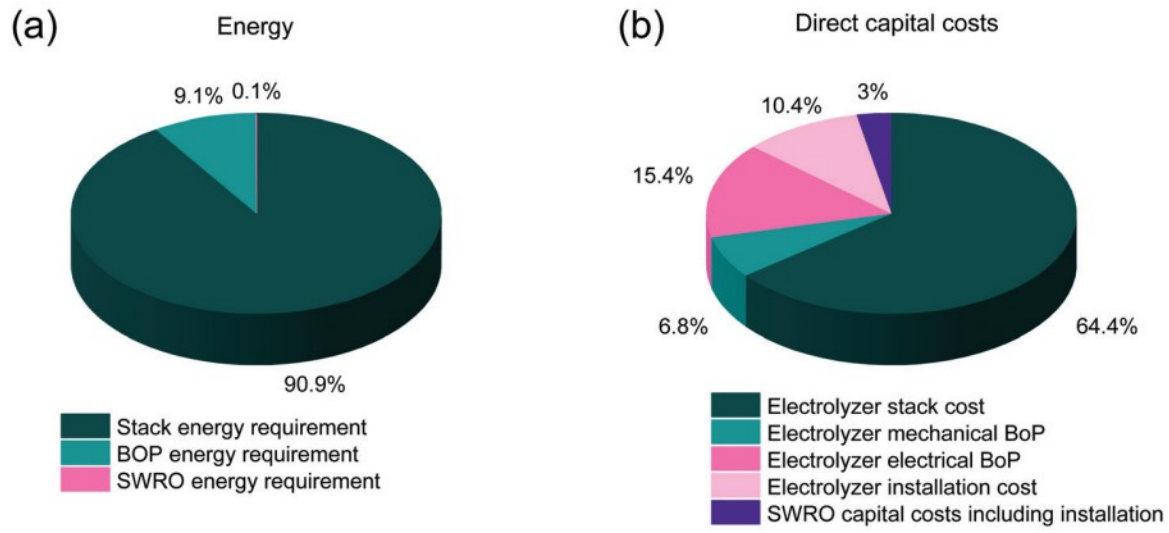

Figure 2.9: Breakdown of a) the energy consumption of a PEM-SWRO system and of b) the capital cost of a PEM-SWRO system [34]

It is likely that the relative cost contribution of the desalination unit will be even smaller in this study, taking into account the wind turbine costs. Therefore, the desalination unit will not be taken into account in the model.

2.2.6.Power electronics

Wind power is an intermittent source, and its conversion into electrical energy is accomplished by the permanent magnet synchronous generator (PMSG) of the direct drive wind turbine. To connect a wind turbine system to the grid, the variable frequency output of the generator must be converted to match the grid frequency. This frequency matching is achieved by a back-to-back converter, comprising a rectifier, a DC-link, and an inverter. Following the alignment of the three-phase connections on both the generator and grid side, the power is reduced from 66 kV to 400 V and transmitted to the grid [35]. Figure 2.10 presents a schematic of a conventional grid-connected wind turbine system.

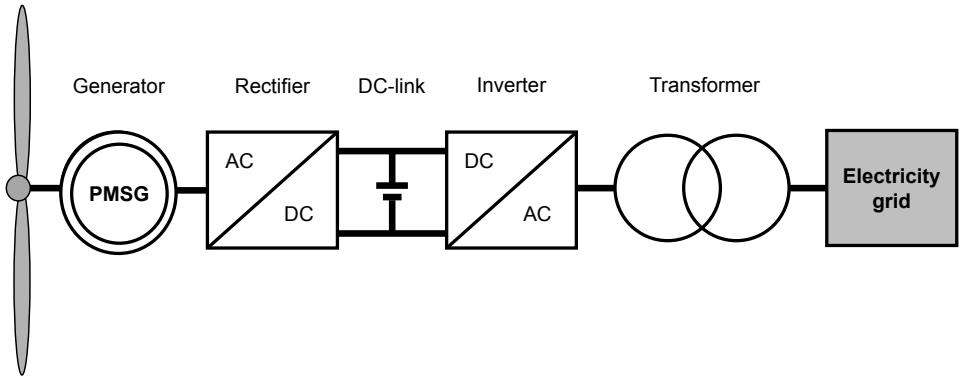

Figure 2.10: A schematic of a conventional grid connected wind turbine system.

ITM Power and Ørsted have proposed a configuration that enables the system components to be directly connected to the DC-link of a wind turbine, thereby reducing the number of power conversion steps, increasing overall efficiency, and reducing the system footprint. This configuration requires redesigning the power electronics of the system components. A future connection schematic between the wind turbine and system components is presented in Figure 2.11, where the voltage is first converted to DC and then stepped down to the desired DC voltage using a buck converter. It is assumed that this configuration can be implemented from 2030 onwards and is accounted for in the model using the specified DC efficiencies of the model components [36], [37].

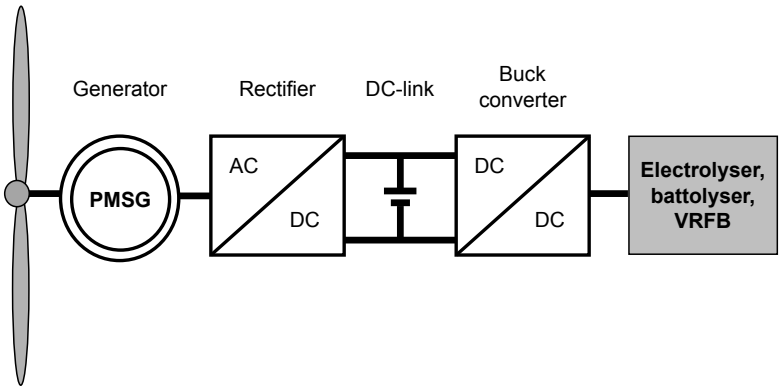

Figure 2.11: A schematic of the future connection between the system components as accounted for in the model [37]

2.3.Structural feasibility

Designing a wind-hydrogen system that includes electrolysis at or in the turbine can pose space and weight constraints. Two options are available for the placement of the hydrogen production components: in the turbine or at the turbine. The model will use a reference turbine of 15 MW to determine the availability of space.

An estimate of the system's footprint must be obtained before exploring potential options. The structural layout of the MC500 PEM electrolyser from NEL Hydrogen, which consists of two containers, is used as a reference. Only the process container is considered for the approximation since the model assumes a direct DC connection between the wind turbine and the hydrogen production system. Assuming that the full wind turbine capacity powers a 15MW electrolyser system, the footprint of the system would consist of six containers, each

approximately 30m^2 and 3 meters tall. The balance of plant of an alkaline electrolyser is generally more complex, resulting in a system footprint about 20% larger than that of PEM [23]. Therefore, the total system footprint for PEM and alkaline technology is estimated to be 180m^2 and 220m^2, respectively. The battolyser footprint is assumed to be equal to that of the alkaline electrolyser.

Now, the feasibility for in-turbine electrolysis will be examined followed by at-the-turbine electrolysis:

In-turbine electrolysis

Due to the length of the containers, it is not space-efficient to fit them into the cylindrical construction of the tower as their length exceeds the diameter of the tower. However, the conditions inside the tower are less harsh than outside, allowing for the electrolyser systems to function properly without being containerized, while retaining the same footprint. The tower has an average diameter of 10 meters in the first 30 meters of height, resulting in a surface area of almost 80m^2 [16]. To account for a service lift, maintenance, and electronic control equipment, a 20% space clearance per floor is taken into consideration, resulting in approximately 65m^2 per floor. For the PEM and alkaline electrolyser systems described in the previous paragraph, 3 and 4 floors, respectively, would be required for the hydrogen production system, assuming desalination takes place underneath the base level of the tower. Considering the height of the containerized system, each floor would take up 3 meters in height, with a maximum height of 15 meters for the alkaline system.

These rough estimates suggest that the required space for in-turbine electrolysis is feasible. Moreover, Siemens Gamesa and Siemens Energy have proposed an example of an in-turbine design, in which the hydrogen production system is fully integrated into the wind turbine tower, as shown in Figure 2.12.

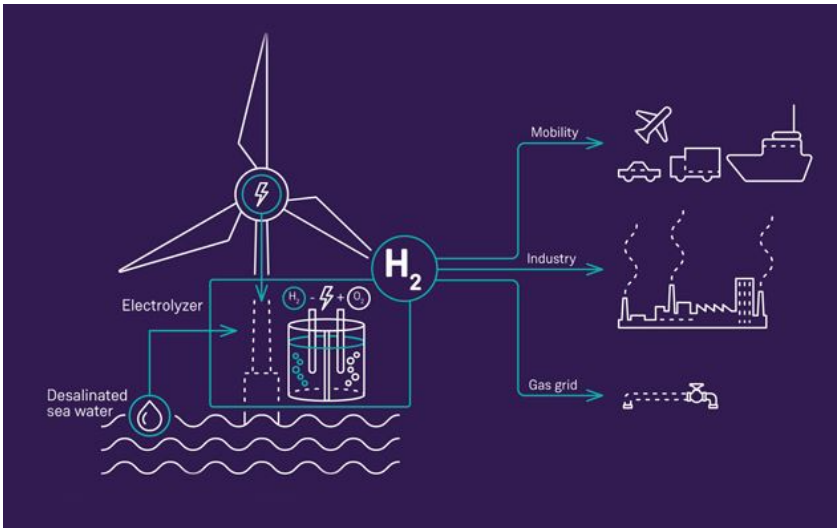

Figure 2.12: Example of an in-turbine electrolysis design and possible hydrogen use cases.

At-the-turbine electrolysis

If space or weight constraints, or other technical difficulties prevent the integration of the hydrogen production system into the wind turbine tower, the system can be placed outside the turbine. H2Dock has developed a standardized, containerized, and modular system that

can be mounted to the base of the wind turbine, reducing the need for offshore engineers and resulting in lower maintenance costs [38]. Figure 2.13 illustrates the H2Dock system.

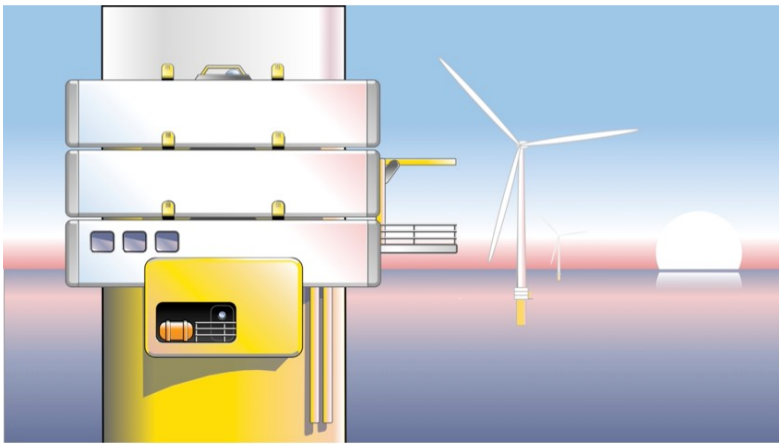

Figure 2.13: A schematic of the future connection between the system components as accounted for in the model.

In conclusion, it can be determined from a structural standpoint that there are ample possibilities to install a hydrogen system either in or at the wind turbine, and that weight and space constraints will not pose significant issues in the future.

3

Methodology

This section details the modeling process employed in this study. It covers the system design configurations, system sizing, implementation of model components in the hydrogen production model, and cost analysis methodology.

3.1.Modelling process

The modelling process in general consists of four parts: identification of the system configurations, the system sizing, the hydrogen production model and the economic analysis. In this section, the four parts of the modelling process are outlined. An overview of the process is shown in Figure 3.1.

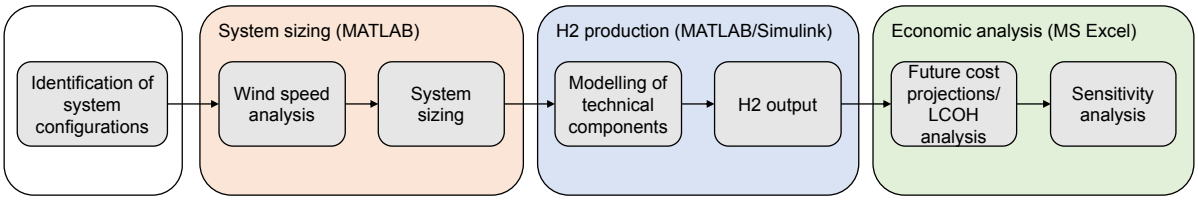

Figure 3.1: A flowchart that shows the modelling process of this research. The colours correspond to the software that is used for the modelling or analysis.

The first step of the modelling process is identifying the system configuration possibilities. The system configurations are introduced in Section 3.2, where it will be clarified what the systems look like, and how the systems are operated.

The next step in the process involves system sizing. The main criterion is ensuring that the battolyser or VRFB can supply enough power and energy to the auxiliary equipment when the wind turbine is not generating power.

As discussed in Section 2.2.1, it is crucial to keep the auxiliary equipment powered at all times for safety reasons and to ensure the wind turbine's longevity. To determine the amount of energy required to power the auxiliary wind turbine equipment, the wind speed analysis calculates the maximum consecutive hours below the cut-in wind speed, which is denoted as Δt_{max}. This value is then used to compute the energy demand of the wind turbine's auxiliary equipment.

The wind speed analysis also computes the frequency of occurrence of a specific duration below the cut-in wind speed. This frequency is related to the number of shutdowns of the electrolyser. This is, because every time the wind speed goes below the cut-in wind speed of the turbine, the electrolyser goes into hot standby mode before shutting down. The frequency of shutdowns increases as the hot standby period (Δt_{sb}) becomes shorter. The electrolyser's lifespan may decrease beyond the maximum number of shutdowns, which is considered

unacceptable in this study. The energy demand of the auxiliary electrolyser equipment is calculated based on Δt_{sb}.

The system is finally sized by installing the maximum electrolyser capacity, where the battolyser or VRFB is still able to fulfill the total auxiliary energy and power demand.

All criteria and assumptions considered during the system sizing process are summarised in the list below:

- The auxiliary wind turbine equipment has to be powered at all times, due to safety reasons and to assure a long wind turbine lifespan.
- The auxiliary equipment of the electrolyser has to be powered during Δt_{sb}.
- The smallest possible value of Δt_{sb} should be calculated to minimise the necessary storage capacity.
- The maximum electrolyser capacity has to be installed, where the battolyser or VRFB is still able to fulfill the total auxiliary energy and power demand.
- The combined electrolyser and storage capacity should equal the wind turbine capacity of 15 MW.
- Both the battolyser and VRFB are expected to be able to discharge over Δt_{max}.

The third step is calculating the amount of hydrogen produced by system, which is highlighted in blue in Figure 3.1. First, the system components are modelled in MATLAB/Simulink. Section 3.4 zooms in on the individual system components. Then, the system sizing results are used as an input to calculate the amount of hydrogen produced.

To analyze the economic viability of the system, the amount of hydrogen produced is used as an input parameter. The economic analysis begins by projecting the future costs of the system components, using a learning curve method explained in Section 3.5. The projected costs are then used to calculate the levelized cost of hydrogen (LCOH) for each system in the analysis. Since the battolyser technology is still relatively new, its capital expenditure (CAPEX) is used as an input variable for LCOH calculation. The analysis compares the different systems, breaks down their LCOH, and conducts a sensitivity analysis. This approach provides a comprehensive understanding of the economic feasibility of the system and allows for informed decision-making.

3.2.System configurations

This section outlines the system configurations evaluated in the study, detailing their design and operation. The configurations considered in the study include an electrolyser-battolyser, an electrolyser-VRFB, and a battolyser-only configuration. These configurations will be used to explain the operational principles of the specific systems.

Electrolyser-battolyser configuration

The electrolyser-battolyser configuration operates by connecting the wind turbine to the battolyser, electrolyser, and desalination unit via a DC-link. Figure 3.2 presents a schematic of this configuration. The wind turbine directly powers the electrolyser, which generates hydrogen. In periods of wind overproduction, excess power is used to charge the battolyser, which produces hydrogen while charging. The maximum hydrogen production rate is achieved when the battolyser is fully charged. During low or no wind, the battolyser stops producing hydrogen and functions as a battery to power the auxiliary components of the system, with the battolyser electricity output denoted as e^-. Seawater is desalinated by the desalination unit and fed into

the electrolyser and battolyser. The operation of the electrolyser-battolyser configuration is depicted in the flowchart in Figure B.1.

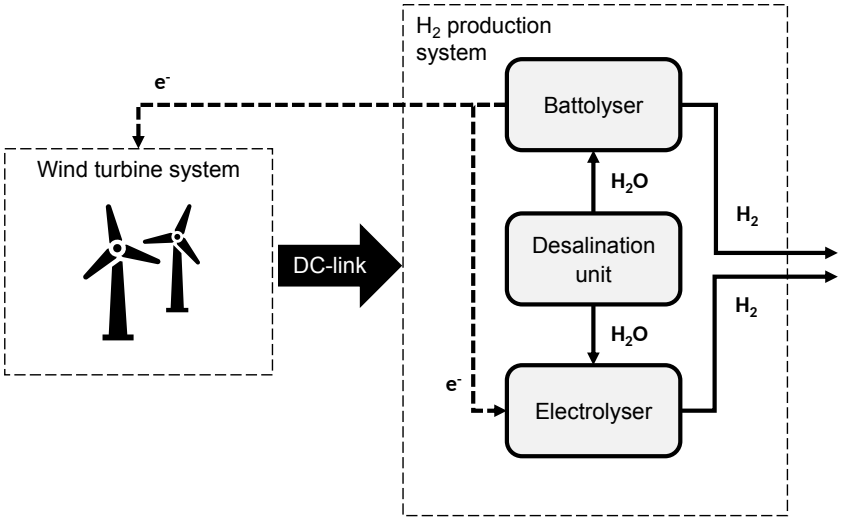

Figure 3.2: An overview of the electrolyser-battolyser configuration, including the streams of substances and electricity. The dashed arrows denote the flows of current to the auxiliary systems when the wind turbine is not producing any power.

Electrolyser-VRFB configuration

In the electrolyser-VRFB configuration depicted in Figure 3.3, the VRFB is used instead of the battolyser. Similar to the electrolyser-battolyser configuration, excess wind turbine power is used to charge the VRFB when the rated capacity of the electrolyser is exceeded. During low or no wind, the VRFB discharges to power the auxiliary components of the system. The operation of the electrolyser-VRFB configuration is illustrated in the flowchart in Figure B.2.

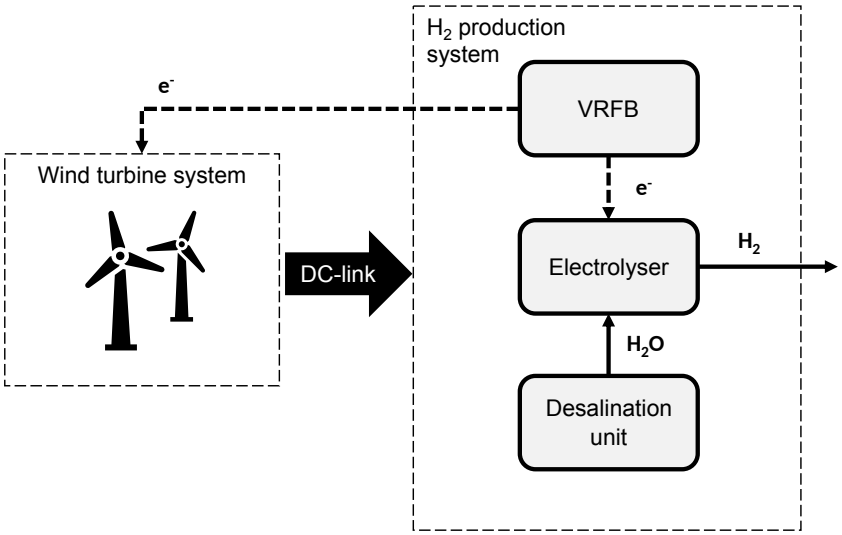

Figure 3.3: An overview of the electrolyser-VRFB configuration, including the streams of substances and electricity. The dashed arrows denote the flows of current to the auxiliary systems when the wind turbine is not producing any power.

Battolyser-only configuration

The battolyser-only configuration utilizes all the power generated by the wind turbine to charge the battolyser. Similar to the electrolyser-battolyser configuration, the battolyser produces hydrogen during charging, reaching the maximum hydrogen production rate when fully charged. As discussed in Section 2.2.3, cold- and hot standby modes are not applicable to the battolyser, and the only auxiliary systems that require power during wind turbine idling are those related to the turbine itself. The flowchart in Figure B.3 provides an overview of the operation of the battolyser-only configuration.

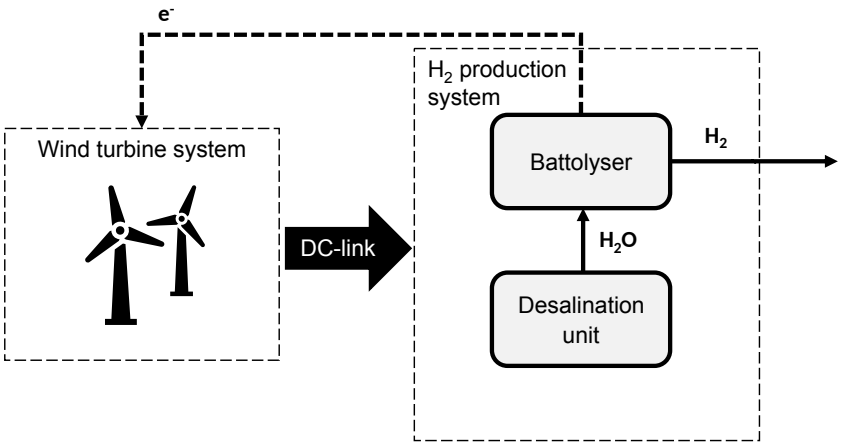

Figure 3.4: An overview of the battolyser-only configuration, including the streams of substances and electricity. The dashed arrow denotes the flow of current to the auxiliary systems when the wind turbine is not producing any power.

Configuration overview

The preceding paragraphs provided a general overview of the three system configurations for illustrative purposes. Based on these configurations, five sub-configurations will be modeled and evaluated, as presented in Table 3.1 along with their corresponding abbreviations for use in the report. The electrolyser-VRFB configuration is further divided into the AEV system and the PEMV system, while the electrolyser-battolyser configuration is subdivided into the AEB system and the PEMB system. The battolyser-only system requires no further division and will be referred to as the B system.

Table 3.1: Overview of the configurations that will be assessed in this study, together with the corresponding abbreviations.

	Configuration	**Abbreviation**
1	Alkaline electrolyser + VRFB	AEV system
2	PEM electrolyser + VRFB	PEMV system
3	Alkaline electrolyser + battolyser	AEB system
4	PEM electrolyser + battolyser	PEMB system
5	Battolyser only	B system

In the following sections the technical model and the implementation of the individual components of the system will be explained in more detail.

3.3.System sizing

Section 3.1 provided a brief overview of the system sizing process. This section will elaborate on the system sizing in more detail, beginning with an analysis of the wind speed profile, followed by an elaboration of the system sizing requirements.

Wind speed analysis

The wind data utilized in the analysis is obtained from an offshore platform located in the North Sea, operated by the KNMI, as reported by [11]. Hourly wind speed data spanning ten years is extracted from a station installed on platform A12CPP, located on the edge of the Dogger Bank in the Dutch EEZ, as it is considered the most representative. Figure 3.5 depicts the location of the platform.

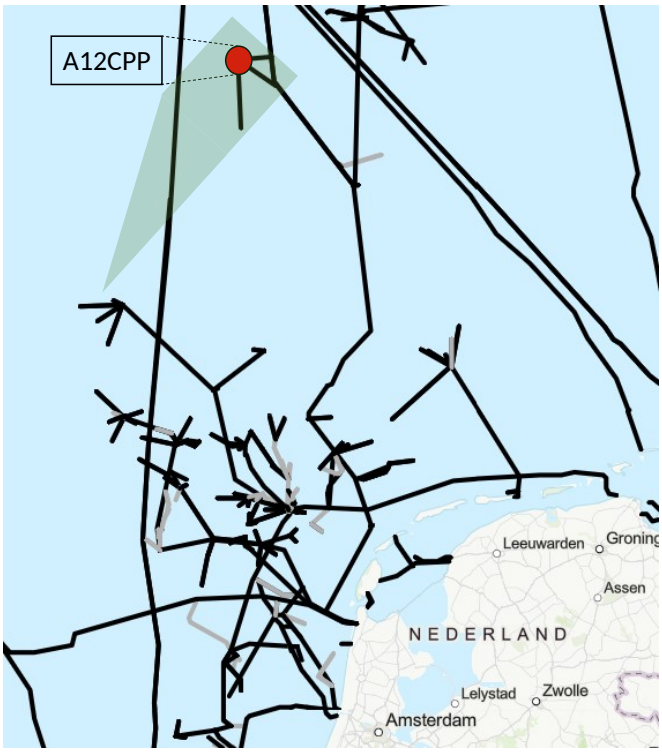

Figure 3.5: The location of the offshore platform and the gas pipeline infrastructure of the North-Sea. The transparent green area represents the Dogger Bank in the Dutch EEZ.

It is assumed that the wind is measured at a height of 50 metres, which is approximately the height of the A12CPP platform. To calculate the wind speeds at hub height, the wind speed is first calculated at 60 metres by using the logarithmic boundary layer law in Equation 3.1. A roughness length of z_0 = 0.0002m for open sea is assumed. [39].

$$U(h) = U\left(h_{ref}\right) \frac{\ln\left(\frac{h}{z_o}\right)}{\ln\left(\frac{h_{ref}}{z_o}\right)} \tag{3.1}$$

As the logarithmic wind profile deviates from the actual wind profile at greater heights, the wind speed at a hub height of 150 metres is calculated using the power law in Equation 3.2. The reference height is taken to be 60 metres, and the power coefficient is assumed to be α = 0.11, as reported in [39].

$$U(h) = U\left(h_{ref}\right)\left(\frac{h}{h_{ref}}\right)^{\alpha} \tag{3.2}$$

The wind speeds calculated by Equation 3.2 are used to calculate the power output of the wind turbine.

The annual wind speed profiles at hub height obtained using MATLAB are utilized to model a distribution using the frequency of observations of each distinct value of Δt. Here, Δt represents a time period of consecutive hours below the cut-in wind speed at hub height. The modelling was conducted for each year of wind speed data, and the average number of observations for each Δt was determined over the years. The resulting distribution is illustrated in Figure 3.6.

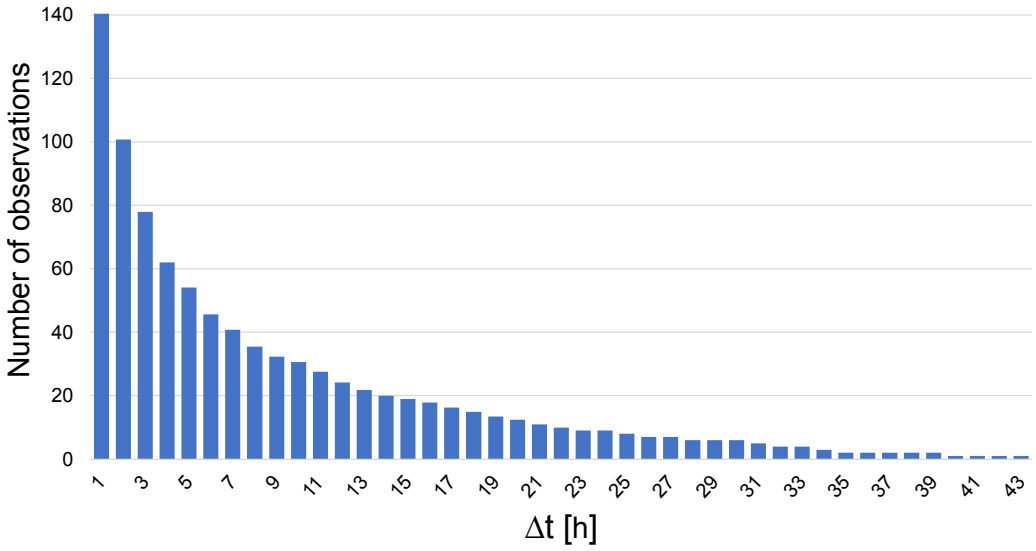

Figure 3.6: The annual frequency of observations of a time period below cut-in windspeed for every Δt_{sb}.

Analysis of Figure 3.6 reveals that the maximum value of Δt is Δt_{max} = 43 hours. As the auxiliary equipment of the wind turbine must operate continuously, Δt_{max} is employed to determine the auxiliary energy demand of the wind turbine.

To compute the auxiliary energy demand of the electrolysers, it is necessary to determine Δt_{sb} of the electrolyser. As Δt_{sb} decreases, the frequency of shutdowns increases. As noted in Section 2.2.2, the maximum number of electrolyser shutdowns can vary from several thousand to 5000, and no definitive manufacturer data are available in the literature. Therefore, a conservative estimate is assumed, with a maximum of 2500 shutdowns during the electrolyser's lifespan.

To ascertain the number of shutdowns at Δt_{sb} = x, one can refer to Figure 3.6 and obtain the number of observations of Δt = x+1. This number of observations of Δt = x+1 equals the number of shutdowns at Δt_{sb} = x, since only values of Δt > x will cause the electrolyser to shut down.

Assuming a value of Δt_{sb} = 1 hour, there are approximately 100 observations (for Δt = 2) where Δt exceeds Δt_{sb}. With a system lifetime of 30 years, this would result in 3000 electrolyser

shutdowns, which exceeds the maximum allowable number of shutdowns. Therefore, Δt_{sb} = 1 hour is not feasible.

On the other hand, for Δt_{sb} = 2 hours, there are 78 observations (for Δt = 3) where Δt exceeds Δt_{sb}. Over a 30-year system lifetime, this would result in 2340 shutdowns, which is within the allowable number of shutdowns. Therefore, Δt_{sb} = 2 hours corresponds to the minimum auxiliary energy demand for the electrolyser.

Sizing requirements

To operate an autonomous offshore wind-hydrogen system, it is necessary to meet the energy and power requirements of the auxiliary systems. The maximum auxiliary energy demand of the wind turbine is equivalent to the auxiliary power demand over a time period of Δt_{max}. Denoting the power demand of the wind turbine as $P_{WT,aux}$, the auxiliary energy demand of the wind turbine is denoted as $E_{WT,aux}$ and is calculated as follows:

$$E_{WT,aux} = P_{WT,aux} \cdot \Delta t_{max} \tag{3.3}$$

To determine the auxiliary energy demand of the electrolyser, the nominal power capacity, $\bar{P}el$, and the minimum load demand of the electrolysers in hot standby mode, θsb, are introduced. Here, θ_{sb} is represented as a percentage of the nominal power capacity. The auxiliary power demand of the electrolyser ($P_{el,aux}$) is obtained by multiplying $\bar{P}el$, θsb. This power demand is then multiplied by Δt_{sb} to yield the auxiliary energy demand. Denoting the auxiliary energy demand of the electrolyser as $E_{el,aux}$, the calculation is expressed as follows:

$$E_{el,aux} = P_{el,aux} \cdot \Delta t_{sb} \tag{3.4}$$

The resulting enery demand that has to be considered in sizing the system is denoted as E_{load}:

$$E_{load} = E_{WT,aux} + E_{el,aux} \tag{3.5}$$

E_{load} is the amount of energy that the battolyser or battery should be able to deliver during Δt_{max}. The required nominal energy capacity of the battolyser is indicated by $\bar{E}_b$, and calculated using Equation 3.6.

$$\bar{E}_b = \frac{E_{load}}{1.45 \cdot \eta_b} \tag{3.6}$$

η_b is the round-trip efficiency of the battery part of the battolyser, specified in Section 3.4.3. The value of 1.45 is the multiplying factor for the capacity of the battery portion of the battolyser, explained in Section 2.2.3. Since the battolyser operates at 1C, the battolyser power capacity can be determined from $\bar{E}_b$.

The required nominal energy capacity of the VRFB is indicated by $\bar{E}_{fb}$, and calculated using Equation 3.6.

$$\bar{E}_{fb} = \frac{E_{load}}{\eta_{fb}} \tag{3.7}$$

η_{fb} is the battery round-trip efficiency, specified in Section 3.4.4.

The maximum power requirement of the auxiliary components is indicated by P_{load}, and calculated using the following equation:

$$P_{load} = P_{WT,aux} + P_{el,aux} \tag{3.8}$$

Finally, the resulting power capacity of the VRFB is:

$$\bar{P}_{fb} = P_{load} \cdot \eta_{fb} \tag{3.9}$$

The system size is determined based on the capacity of the electrolyser. As the electrolyser capacity increases, the total auxiliary energy demand also increases. The maximum electrolyser capacity is computed by ensuring that the battolyser or VRFB is capable of supplying the required energy and power to the auxiliary components. When it is no longer possible to increase the electrolyser capacity without violating this condition, the system sizing process is complete.

3.4.Model implementation

3.4.1.Wind turbine

Table 3.2 presents the technical and physical parameters of the 15 MW reference turbine [16]. In the future, wind turbines are expected to increase in size and distance from shore, resulting in higher capacity factors. Furthermore, more turbines will be installed in deeper waters, increasing the proportion of floating foundations. In this study, the same location and reference turbine with a monopile foundation are used for both the 2030 and 2050 scenarios, implying that the technical parameters remain unchanged. However, ongoing development of wind turbine components is expected to enhance their robustness and extend their lifespan. Specifically, the lifetime of the wind turbine is assumed to be 25 and 30 years in 2030 and 2050, respectively.

Table 3.2: Technical wind turbine parameters

Parameter	Unit	Value	Ref.
Hub height, h_{hub}	m	150	[16]
Rotor radius, R	m	120	[16]
Rated power. P_{rated}	MW	15	[16]
Hot standby power demand, $P_{WT,aux}$	kW	100	[19]
Cut-in wind speed, U_{in}	m/s	3	[16]
Rated wind speed, U_{rated}	m/s	11	[16]
Cut-out wind speed, U_{out}	m/s	25	[16]

The power output of the wind turbine incorporated in the technical model is mathematically expressed by Equation 3.10. Here, U_{hub} denotes the wind speed at hub height, and ρ represents the air density, which is assumed to have a value of ρ = 1.225 kg/m^3.

$$P_{WT}(t) = \begin{cases} 0, & 0 < U(t) < 3 \\ \frac{1}{2} \cdot \rho \cdot \pi \cdot R^2 \cdot U_{hub}(t)^3 \cdot C_{p,max}, & 3 < U(t) < 11 \\ 15, & 11 < U(t) < 25 \\ 0, & 25 < U(t) < \infty \end{cases} \tag{3.10}$$

The power coefficient C_p is the ratio of the power extracted by the wind turbine and the available energy in the incoming wind stream. The value of C_p is variable as it depends on the incoming wind speed. During operation it is assumed that control optimises power production. To be able to calculate the power output of the wind turbine, the maximum value for the power coefficient is taken throughout the entire operation. The maximum power coefficient, $C_{p,max}$, can be determined by rewriting Equation 3.10 and by using P_{rated} and U_{rated} as an input. This results in $C_{p,max}$ = 0.41.

3.4.2.Electrolysers

Table 3.3 presents the estimated technical parameters for the electrolyser technologies in 2030 and 2050.

Table 3.3: Technical parameters for AE and PEM in 2030 and 2050.

Parameter	Unit	2030	2050	Ref.
AE				
Lifetime (stack), $LT_{stack,AE}$	hours	100000	125000	[40] [41] [23]
DC Efficiency (stack), $\eta_{stack,AE}$	% of HHV	85	87.5	[42] [23]
Stack degradation, $\eta_{sd,AE}$	%/1000h	0.10	0.08	[43]
Minimum load, $\theta_{min,AE}$	%	10	5	[23]
Hot standby load, $\theta_{sb,AE}$	%	2	2	
Operating temperature, $T_{el,AE}$	°C	60	60	[41] [44]
Operating pressure, $p_{el,AE}$	bar	30	30	[41] [44]
PEM				
Lifetime (stack), $LT_{stack,PEM}$	hours	90000	125000	[40] [41]
DC Efficiency (stack), $\eta_{stack,PEM}$	% of HHV	82	87.5	[45] [23]
Stack degradation, $\eta_{sd,PEM}$	%/1000h	0.12	0.08	[43]
Minimum load, $\theta_{min,PEM}$	%	5	5	[23]
Hot standby load, $\theta_{sb,PEM}$	%	2	2	
Operating temperature, $T_{el,PEM}$	°C	60	60	[41] [45]
Operating pressure, $p_{el,PEM}$	bar	30	30	[41] [46]

The estimates are partially based on estimates from renowned institutions and partially on the following assumptions.

- η_{stack} is based on the most progressive data from various commercially available large-scale electrolysis systems. $\eta_{stack,AE}$ data varies between approximately 82%-85% based

on operating conditions. A progressive value of 85% is assumed for the 2030 scenario. $\eta_{stack,PEM}$ data varies between approximately 79%-82% and a progressive value of 82% is assumed.

- The way of measuring minimum operating loads may vary between manufacturers as the minimum operating loads are far apart for various manufacturers. The most progressive values were assumed for θ_{min} in the 2030 scenario.
- The targets for the system availability factor, η_{sd}, have been adjusted for both the AE- and PEM-system between 2020 and 2030. The target for $\eta_{sd,AE}$ has decreased from 0.12 to 0.10 %/1000h, while the target for $\eta_{sd,PEM}$ has decreased from 0.19 to 0.12 %/1000h. It is assumed that there will be a further decrease of 0.02 and 0.04, respectively, resulting in a target of 0.08 %/1000h by 2050 for both systems.
- The values for the 2050 scenarios for the AE and PEM are the same. This can be attributed to the fact that the AE-system is a more established technology and therefore has a lower potential for improvement compared to the PEM-system, which is a newer technology with more room for enhancement. Hence, both systems are expected to converge towards similar technical performance levels by 2050.

Operating mode

In operating mode the electrolysers are operating at or above minimum load and producing hydrogen. P_{el} is the available power for hydrogen production, represented by Equation 3.11.

$$P_{el}(t) = \begin{cases} 0, & P_{WT,el}(t) < \bar{P}_{el} \cdot \theta_{min} \\ P_{WT,el}(t) \cdot \eta_{el}(t), & \bar{P}_{el} \cdot \theta_{min} < P_{WT,el}(t) < \bar{P}_{el} \cdot \theta_{max} \\ \bar{P}_{el} \cdot \eta_{stack,el}(t), & \bar{P}_{el} \cdot \theta_{max} < P_{WT,el}(t) \end{cases} \tag{3.11}$$

The power produced by the electrolyser is denoted as P_{el} and is calculated using the nominal power capacity of the electrolyser, $\bar{P}el$, and the upper boundary of the load range, θmax (assumed to be 100%). $P_{WT,el}$ is the power produced by the wind turbine dedicated to the electrolyser, which is limited by the operating range of the electrolyser. The excess wind turbine power is used to charge the battolyser. The efficiency losses are accounted for using the system efficiency of the electrolyser, denoted as η_{el} and calculated using Equation 3.12.

$$\eta_{stack,el}(t) = \eta_{pl,el} \cdot \eta_{sd,avg} \tag{3.12}$$

where $\eta_{sd,avg}$ is the averaged yearly stack degradation, which accounts for stack replacements throughout the lifetime of the system. $\eta_{pl,el}$ is the partial load efficiency of the electrolyser, which has a characteristic shape for various electrolyser technologies.

The partial load efficiency curves of the electrolysers are determined by the voltage efficiency and Faraday efficiency curves, as explained in Section 2.2.2. These curves are based on a reference model introduced by Sánchez et al. (2020) [47], which takes into account temperature (60°C) and pressure (30 bar). The model was originally created to simulate the characteristics of AE, but studies have used it to describe PEM performance as well [48]. The fundamental model was created by Ulleberg (2003) [49].

The Faraday efficiency curve from the reference model was directly implemented, but the voltage efficiency was deemed too low. To achieve the desired DC efficiency at full load, a new voltage curve was created using the characteristic form of the reference curve. This

involved fitting a power curve ($y = ax^b$) over the reference curve and using this information to produce a new voltage curve with similar characteristics. The product of the voltage efficiency and Faraday efficiency resulted in a new partial load curve that achieves the desired DC efficiency at full load. The new partial load curves are taken into account in the Simulink model to accurately describe the electrolyser performance in intermittent operation. The resulting efficiency curves for AE and PEM in 2030 and 2050 are presented in Figure 3.7 and 3.8.

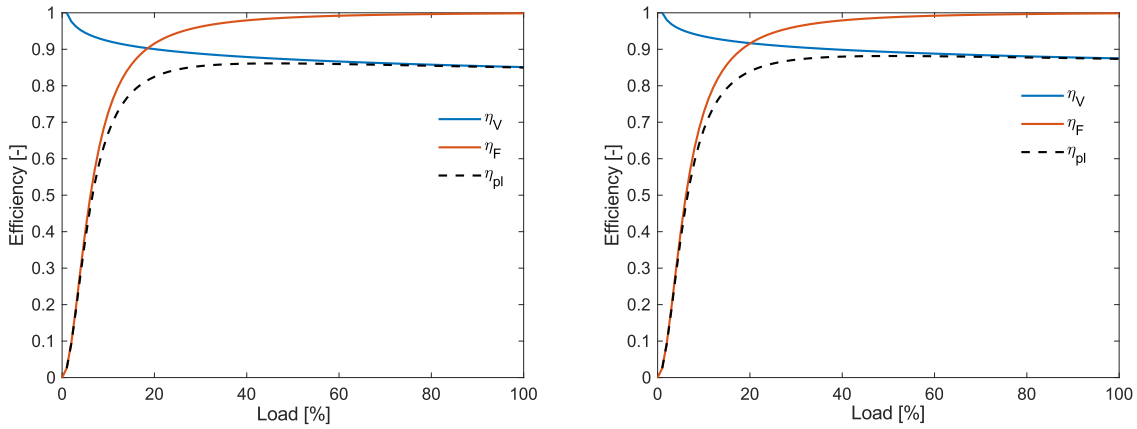

(a) AE 2030 **(b)** AE 2050

Figure 3.7: The voltage efficiency, Faraday efficiency and partial load efficiency curves for alkaline electrolysis in a) 2030 and b) 2050.

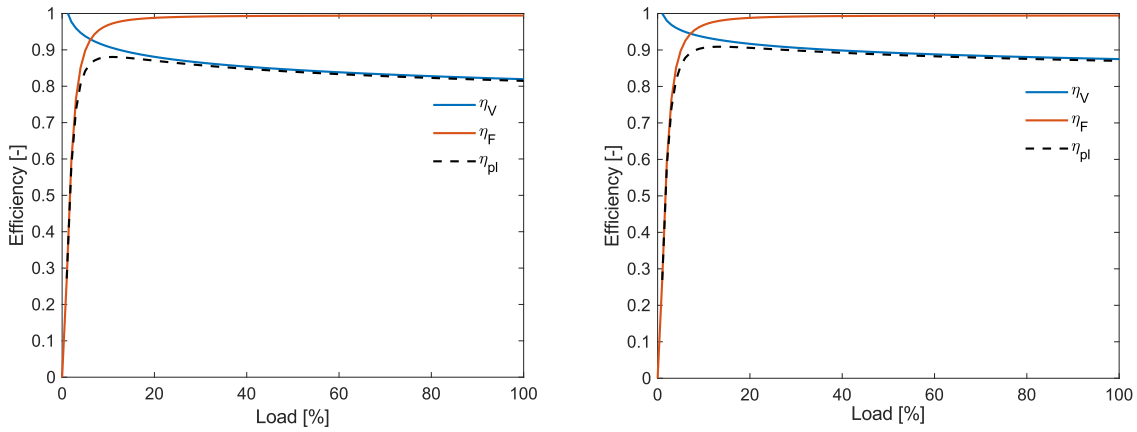

(a) PEM 2030 **(b)** PEM 2050

Figure 3.8: The voltage efficiency, Faraday efficiency and partial load efficiency curves for PEM electrolysis in a) 2030 and b) 2050.

The rate at which hydrogen is being produced (kg/h) is calculated using Equation 3.13.

$$\dot{m}_{H_2,el}(t) = \frac{P_{el}(t)}{HHV_{H_2}} \tag{3.13}$$

HHV_{H_2} is the higher heating value of hydrogen, being equal to 39.4 kWh/kg. To calculate the amount of hydrogen produced in a year, the integral is taken over the available power produced in a year

Hot standby mode

Section 2.2.2 describes the auxiliary power demand of electrolysers, assuming that the power demand during hot standby mode is 2% of the nominal power capacity for both 2030 and 2050 scenarios [50]. The power demand is represented by P_{load} and calculated using Equation 3.14.

$$P_{load,el}(t) = \begin{cases} 0, & \bar{P}_{el} \cdot \theta_{min} < P_{WT,el}(t) \\ \theta_{sb} \cdot \bar{P}_{el}, & P_{WT,el}(t) < \bar{P}_{el} \cdot \theta_{min} \end{cases} \tag{3.14}$$

3.4.3.Battolyser

The technical parameters of the battolyser for the 2030 and 2050 scenario are listed in Table 3.4 below.

Table 3.4: Technical parameters for the battolyser in 2030 and 2050.

Parameter	Unit	2030	2050	Ref.
Battolyser (battery)				
Battery efficiency (round-trip), $\eta_{b,b}$	%	80	80	[30]
Battery range. $\theta_{min,b}$ - $\theta_{max,b}$	%	0-145	0-145	[30]
Maximum C-rate	[-]	1C	1C	
Battolyser (electrolysis)				
Lifetime (stack), $LT_{stack,b}$	hours	100000	125000	Table 3.3
DC Efficiency (stack), $\eta_{stack,b}$	% of HHV	85	87.5	Table 3.3
Stack degradation, $\eta_{sd,b}$	%/1000h	0.10	0.08	Table 3.3
Minimum load, $\theta_{min,b}$	%	0	0	[30]
Operating temperature, T_b	°C	60	60	Table 3.3
Operating pressure, p_b	bar	30	30	Table 3.3

The following assumptions were made regarding the technical parameters of the battolyser:

- Because the battolyser is a new technology, it is difficult to make statements about the future efficiency of the battery part. If you only look at the Ni-Fe battery, there are other technologies that have more potential. Therefore, few studies have been done on the future parameters of Ni-Fe batteries. Keeping the efficiency the same also keeps the system sizing the same for the 2030 and 2050 scenario
- Considering the robustness of Ni-Fe batteries and their resilience against deep discharges, $\theta_{min,b}$ is assumed to be 0%. The increased $\theta_{max,b}$ of 145% is related to usage of extra electrode material, explained in Section 2.2.3.
- The electrolysis portion of the battolyser is comparable with AE. Therefore the same values are assumed for LT_{stack}, η_{stack}, η_{sd}, T_{el}.
- The battolyser has no minimum operating load, as no safety issues occur at low loads, which is inherent to battolyser technology.

- At ambient temperatures, Ni-Fe batteries have a relatively high self-discharge rate of 1-2% per day [51]. At higher temperatures self-discharge could even reach 8 to 10% per day [51]. However, the due to the connection with an intermittent power source, the battolyser is being charged frequently. Additionaly, Figure 3.6 shows that the number of observations for high values of Δt (> 12h) is relatively low. Therefore the self-discharge of the battery is not taken into account in the model.
- It is assumed that there is no minimum discharge rate.

Battolyser operation

Figure 3.9 provides a summary of the battolyser operation in the AEB and PEMB systems, depicting the control flow chart.

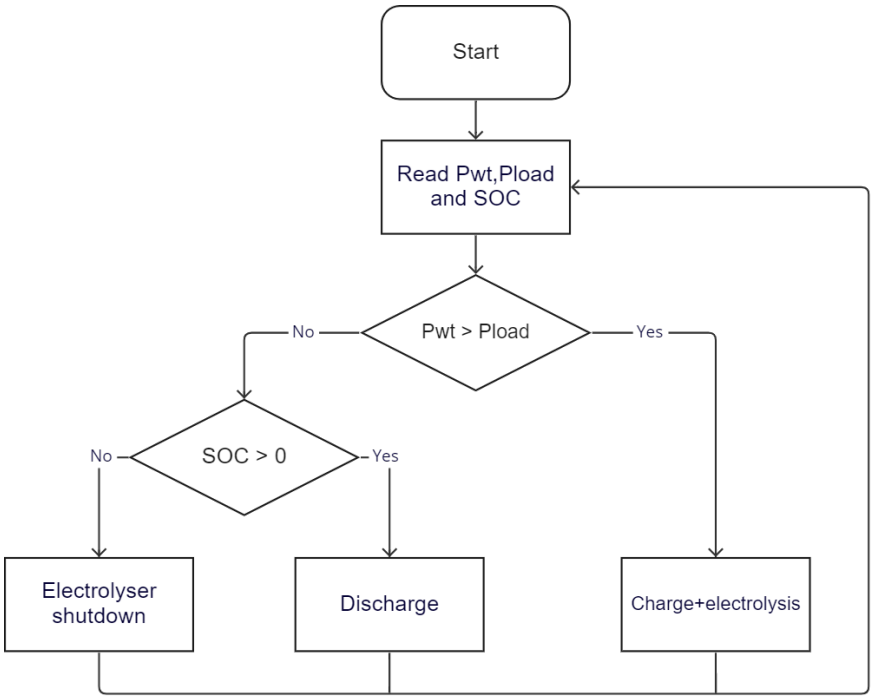

Figure 3.9: Flowchart that describes the battolyser operation in the AEB system and PEMB systems

The SOC of the battery is determined by dividing the amount of energy in the battery at a given time (E_b) by the total energy capacity ($\bar{E}_b$), which is computed in Equation 3.15.

$$SOC(t) = \frac{E_b(t)}{\bar{E}_b} \tag{3.15}$$

According to the system sizing of the system in Section 3.3, the total energy capacity of the battolyser is enough to keep the electrolyser in hot standby mode for a time period of Δt_{sb}. Thereafter, the battery is empty and the electrolyser shuts down.

In the B system, there is no electrolyser to shut down. This results in the control flow chart presented in Figure 3.10. In this system, the SOC is only relevant for determining the partial load efficiency of the battolyser. Dynamic charge and discharge efficiencies are not implemented in the model. Instead, a static round-trip efficiency is implemented and accounted for in the initial sizing of the system.

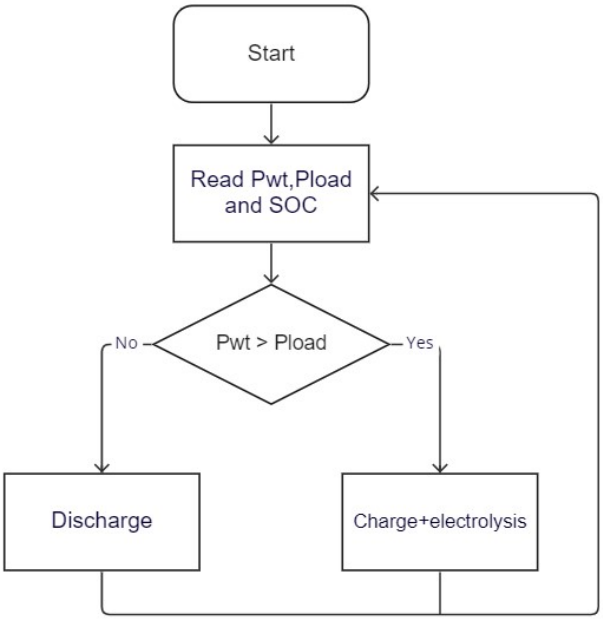

Figure 3.10: Flowchart that describes the battolyser operation in the B system

Battery output

The output power of the battery portion, $P_{b,b}$ is represented by Equation 3.16

$$P_{b,b}(t) = \begin{cases} P_{load}(t), & P_{WT,b}(t) < P_{load}(t) \\ 0, & P_{WT,b}(t) > P_{load}(t) \end{cases} \tag{3.16}$$

For the AEB system and PEMB system, P_{load} is equal to the sum of $P_{WT,aux}$ and $P_{el,aux}$. For the B system, P_{load} equals $P_{WT,aux}$ as there are no electrolysers in the B system.

Electrolysis output

The available power for hydrogen production for the battolyser is indicated by P_b, calculated in Equation 3.17.

$$P_{b,el}(t) = \begin{cases} 0, & P_{WT,b}(t) < P_{load}(t) \\ P_{WT,b}(t) \cdot \eta_{stack,b}(t) \cdot F_{b,el}, & P_{WT,b}(t) > P_{load}(t) \end{cases} \tag{3.17}$$

where $P_{WT,b}$ is the portion of power produced by the wind turbine that is going to the battolyser. $F_{b,el}$ is the charge utilisation factor for electrolysis, explained in Section 2.2.3. $\eta_{stack,b}$ is the stack efficiency of the battolyser calculated in Equation 3.18.

$$\eta_{stack,b}(t) = \eta_{pl,b} \cdot \eta_{sd,avg} \tag{3.18}$$

As outlined in Section 2.2.3, the partial load efficiency of the battolyser, $\eta_{pl,b}$, is the product of the voltage efficiency and Faraday efficiency. However, experimental findings indicate that the Faraday efficiency of the battolyser is 100%, with an accuracy of 0.5% [30]. Consequently, it is assumed that the Faraday efficiency is 100% in the model. Thus, the partial load efficiency $\eta_{pl,b}$ is equivalent to the voltage efficiency across the entire load range.

The voltage efficiency of the battolyser is derived from experiments conducted by Mulder et al. (2017) using a 10Ah battolyser [30]. Figure 3.11 depicts the Tafel plot of the battolyser's voltage potential versus the applied current, as per the experiments carried out by Mulder et al. (2017) [30].

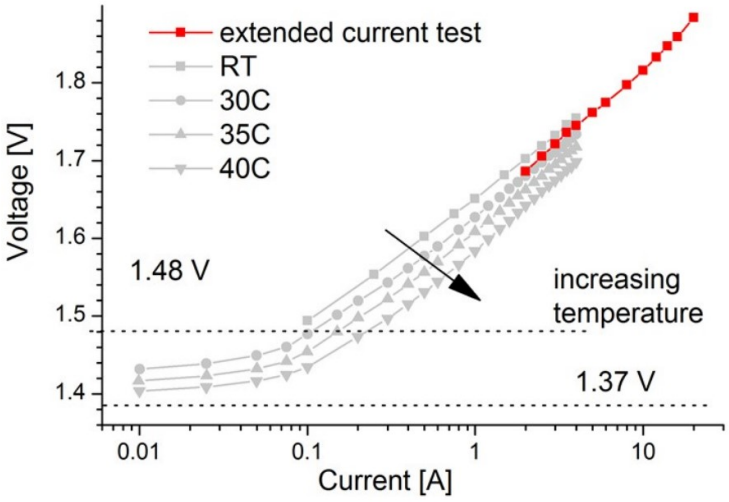

Figure 3.11: Tafel plot of the potentials reached by the battolyser during electrolysis [30]

In the model of this study, a maximum charge rate of 1C is assumed, which means that the maximum cell potential is reached at 10A. According to Figure 3.11, 10A corresponds to a cell potential of 1.82V or a voltage efficiency of 81%.

To generate the voltage efficiency curves for the 2030 and 2050 scenarios, the process employed in producing the voltage efficiency curve for the electrolysers, as described in Section 3.4.2, was also utilized for the battolyser. This resulted in the voltage efficiency curves presented in Figure 3.12.

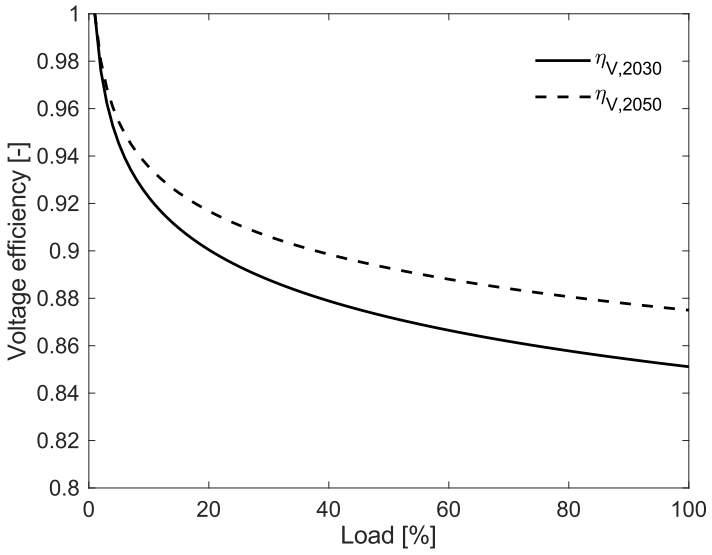

Figure 3.12: Voltage efficiency curve resulting from the Tafel plot that describes the battolyser

The resulting hydrogen production rate by the supporting battolyser is indicated by $\dot{m}_{H_2,b}$ and calculated in Equation 3.19.

$$\dot{m}_{H_2,b}(t) = \frac{P_b(t)}{HHV_{H_2}} \tag{3.19}$$

3.4.4.Vanadium redox flow battery

Table 3.5 presents the technical parameters of the VRFB that are used in the hydrogen production model.

Table 3.5: Technical parameters for the battolyser in 2030 and 2050.

Parameter	Unit	2030	2050	Ref.
Battery efficiency (round-trip), η_{fb}	%	83	83	[52]
Battery range. $\theta_{min,fb}$ - $\theta_{max,fb}$	%	0-100	0-100	[52]
Lifetime. LT_{fb}	years	25	30	[53]

With regard to the technical parameters, the following assumptions were made:

- For the battery part of the battolyser, the round-trip efficiency was kept the same for the 2030 and 2050 scenario. To make a fair comparison between the electrolyser-battolyser and electrolyser-VRFB configurations, the battery efficiency of the VRFB is kept the same as well.
- Manufacturers currently report battery lifetimes of 25+ years and a cycle life of >20000 cycles. It is assumed that VRFB's will reach a 30 year lifetime by 2050.
- It is assumed that there is no minimum discharge rate.

VRFB operation

The VRFB operation is similar to the operation of the battery portion of the battolyser. Therefore, the VRFB operation can be described by the flowchart in Figure 3.9, but without electrolysis. The output power of the VRFB, P_{fb} is represented by Equation 3.20

$$P_{fb}(t) = \begin{cases} P_{load}(t), & P_{WT,b}(t) < P_{load}(t) \\ 0, & P_{WT,b}(t) > P_{load}(t) \end{cases} \tag{3.20}$$

For the AEV system and PEMV system, P_{load} is equal to the sum of $P_{WT,aux}$ and $P_{el,aux}$.

3.5.Cost analysis

The learning curve method

Future cost estimations are made based on a commonly applied single-factor learning curve (SFLC) method, first introduced by T.P. Wright (1936) [54]. This SFLC-method assumes a specific cost reduction rate (learning rate) with every doubling of cumulative installed capacity. Taking cumulative installed capacity as cost reduction driver is referred to as 'learning-by-doing'. According to this method, the estimated $CAPEX$ of a technology in a specific year can be described by Equation 3.21:

$$CAPEX_t = CAPEX_0 \cdot \left(\frac{CAP_t}{CAP_0}\right)^{\varepsilon} \tag{3.21}$$

, where $CAPEX_t$ are the capital expenditures of a technology in year t at a cumulative installed capacity of CAP_t. $CAPEX_0$ are the capital expenditures at time $t = 0$ at a cumulative installed capacity of CAP_0. ε is the experience parameter of which the relation with the learning rate (LR) is described by Equation 3.22 [55]:

$$LR = 1 - 2^{\varepsilon} \tag{3.22}$$

This study's various learning rates are based on literature and assumptions, which will be clarified in the sections hereafter. Using these learning rates, the experience parameter (ε) can be determined and subsequently used to calculate $CAPEX_t$.

For the future CAPEX estimations, the single-factor learning curve method was used. However, more complex methods to estimate future cost trajectories are implementing multi-factor learning curves (MFLC) and bottom-up approaches. The MFLC method assumes multiple drivers for cost reduction, for example, learning by doing and learning by interacting across different stakeholders and geographical areas [56]. In a bottom-up approach, the cost of a technology is expressed as the sum of its sub-components. Then, the sub-components are analysed through specific cost functions. The limitation of the above-described methods is that a lot of detailed data is required. For instance, cost data of electrolyser components has yet to be readily available due to confidentiality, and potential competitive advantages [57]. Therefore, the more straightforward SFLC method was applied in this study.

LCOH calculation

The total cost of hydrogen production in euros per kilogram is defined by the levelised cost of hydrogen ($LCOH$). To calculate the LCOH, several cost equations will be introduced first.

The total capital expenditures for the various system configurations are defined by the following equations:

$$CAPEX_{total,elec-batto} = CAPEX_{WT} + CAPEX_{el} + CAPEX_b \tag{3.23}$$

$$CAPEX_{total,elec-VRFB} = CAPEX_{WT} + CAPEX_{el} + CAPEX_{fb} \tag{3.24}$$

$$CAPEX_{total,b-only} = CAPEX_{WT} + CAPEX_b \tag{3.25}$$

, where $CAPEX_{WT}$ is the wind turbine CAPEX and $CAPEX_{el}$ is the electrolyser CAPEX, which includes the cost of stack replacement. $CAPEX_{fb}$ is the CAPEX of the VRFB. As mentioned in Section 2.2.5, the desalination unit CAPEX is negligible.

As the battolyser is still in its infancy, no direct cost data is available. Therefore, instead of estimating the battolyser CAPEX ($CAPEX_b$) based on assumptions, $CAPEX_b$ is used as an input variable. By using $CAPEX_b$ as an input variable, the relation between $CAPEX_b$ and the system LCOH can be analysed.

To obtain the annualised CAPEX ($CAPEX_{total/yr}$, $CAPEX_{total}$ is distributed along the lifetime of a project to determine the yearly spent CAPEX. This is done by multiplying it with a dimensionless annuity factor (AF). This factor is calculated using Equation 3.26:

$$AF = \frac{(1+r)^t \cdot r}{(1+r)^t - 1} \tag{3.26}$$

Costs can be divided into initial investments and those incurred during the lifetime of a system. Discounting is necessary to account for decreased monetary value over time due to interest accrual and inflation. By discounting, investors gain insight into the anticipated future worth of an investment. The discount factor, denoted by r, is based on the weighted average cost of capital (WACC), which measures the expected rate of return required by investors to finance a company's equity and pay off its debt.

ORE Catapult suggests that a WACC of 6% is appropriate for a bottom-fixed offshore wind project [58], which could decrease to approximately 4% by 2040 [59]. On the other hand, for electrolysers in conjunction with onshore wind, a WACC of 10% is currently expected, but this could potentially decline to 6% in the future [23]. For both the 2030 and 2050 scenarios, the cost analysis employs a WACC of 6%. The sensitivity analysis in Section 4.6 accounts for possible variations in the WACC.

Operational expenditures are fixed OPEX ($OPEX_{fix}$) and variable OPEX ($OPEX_{var}$), which include expenses for unplanned maintenance, electricity, and water procurement. However, as the system design uses seawater and is self-contained, $OPEX_{var}$ is not relevant. Therefore, $OPEX_{fix}$ represents $OPEX_{total}$. The calculation of $OPEX_{total}$ for different system configurations is performed using the given equations.

$$OPEX_{total,elec-batto} = OPEX_{WT} + OPEX_{el} + OPEX_b \tag{3.27}$$

$$OPEX_{total,elec-VRFB} = OPEX_{WT} + OPEX_{el} + OPEX_{fb} \tag{3.28}$$

$$OPEX_{total,b-only} = OPEX_{WT} + OPEX_b \tag{3.29}$$

The OPEX of each component are calculated as a percentage of the corresponding CAPEX. These percentages ($OPEX_{WT,\%}$, $OPEX_{PEM,\%}$,$OPEX_{AE,\%}$ and $OPEX_{VRFB,\%}$) and the reasoning behind it are explained in Sections 3.5.1, 3.5.2 and 3.5.3. $OPEX_{bat}$ is calculated using the same percentages used for calculating $OPEX_{el}$.

Using Equations 3.25 - 3.29, the LCOH can be calculated through Equation 3.30.

$$LCOH = \frac{((CAPEX_{total} \cdot AF) + OPEX_{total})}{\dot{m}_{H_2,total}} \tag{3.30}$$

3.5.1.Wind turbine

Cost parameters

Table 3.6 displays the current cost structure of a wind turbine, as determined by Offshore Renewable Energy (ORE) Catapult through a detailed analysis. The data refers to a 1GW

project comprising of one hundred 10MW wind turbines installed in a water depth of 30m. ORE Catapult considers the cost data to be applicable for wind farms built until 2025 [58]. However, ORE Catapult's analysis assumes a scenario where wind turbine-generated electricity is transported to the mainland, and thus, the installation and commissioning of on- and offshore cables and substations have significant cost implications.

Table 3.6: Wind turbine cost based on ORE Catapult data for the year 2022 [58]

Category	**Rounded cost (€/kW)**
Development and project management	140
Turbine	1170
Balance of plant (BoP)	330
Installation and commissioning	430
O&M (per annum)	70
Decommissioning	90
Total OPEX	**70**
Total CAPEX	**2160**

The study omits certain cost items that are irrelevant to the researched system design, leading to a 29% reduction in OPEX and a 34% reduction in CAPEX compared to a typical wind farm. Figure B.4 provides a comprehensive breakdown of the cost items by category, including those that were discarded. The decommissioning costs are calculated using a project lifespan of 25 years, consistent with the ORE Catapult study (WTcatapult).

The assumed specific learning rates, installed capacities, and starting point CAPEX for the 2030 and 2050 scenarios are presented in Table 3.7.

Table 3.7: Economic parameters for the wind turbine for the years 2030 and 2050

Parameter	**Unit**	**2030**	**2050**	**Ref.**
Learning rate, LR_{WT}	%	10	5	[60] [61] [55]
Cum. installed capacity, CAP_{WT}	GW	250	1100	[62] [63]
OPEX, $OPEX_{WT,\%}$	%	3	2	[64]

The literature reports a range of learning rates, spanning from below 5% to above 30% [60], [61]. However, a study conducted by the Joint Research Centre (JRC) Europe indicates that the majority of data falls within the 5%-20% range [55]. Learning rates tend to decrease over time as technology matures and deployment costs decrease. This study assumes a current learning rate of 15% and projects a decrease to 10% in 2030 and 5% in 2050.

Due to the distinct technology used in floating and fixed-bottom foundations for offshore wind, the cumulative installed capacity for floating offshore wind is excluded from calculations. The learning rate of floating offshore wind is expected to be higher due to its less established nature. Additionally, it is projected that the cumulative installed capacity of floating offshore wind will grow exponentially towards 2050 [65]. Including floating offshore wind capacity would lead

to inaccurately lower OPEX and CAPEX, as the wind turbine foundation is a significant cost driver.

The current cumulative installed capacity of offshore wind energy globally stands at approximately 60 GW [62]. According to McKinsey Company's analysis, the cumulative installed capacity is anticipated to grow to around 200 GW in 2030 and nearly 650 GW in 2050 in the base case scenario [63]. The accelerated scenario predicts values of 265 GW in 2030 and 1240 GW in 2050, both including floating offshore wind. Floating offshore wind is expected to comprise approximately 4% of the total in 2030 and 15% in 2050 [65]. Fixed-bottom offshore wind is estimated to have capacities of 385 GW in 2030 and 1700 GW in 2050, according to DNV's report. By averaging the figures above and excluding floating offshore wind, the projected installed capacity is estimated to be 250 GW in 2030 and 1100 GW in 2050, which is used in the model.

The initial OPEX is 3.2% of the wind turbine CAPEX, according to the data in Table 3.6. It is assumed that the OPEX will decrease to 3% in 2030 and 2% in 2050 [64].

3.5.2.Electrolysers

Cost parameters

The Fraunhofer institute conducted a bottom-up analysis, which presented a cost breakdown for a 5 MW AE and PEM electrolyser, shown in Figure B.5. The study excluded costs associated with mechanical compression and power electronics due to the specific system design. Additionally, housing costs were not considered, as it was assumed that housing refers to more than just a containerized system. Consequently, these costs were deducted from the balance of plant (BoP) costs. This led to a 22% cost reduction for PEM and a 32% cost reduction for AE. The higher cost reduction for AE is attributed to the fact that the reference study did not include compression for PEM. [57]

The CAPEX and OPEX in Table 3.8 are used as the starting point for the future cost analysis.

Table 3.8: Cost breakdown of the AE and PEM electrolyser for various categories and the resulting OPEX and CAPEX [57]

Category	**AE (€/kW)**	**PEM (€/kW)**
Electrolysis stacks	185	295
Balance of plant (BoP)	465	470
Total OPEX	**15**	**25**
Total CAPEX	**650**	**765**

Table 3.8 shows that the stacks contribute to 30% and 40% of the total CAPEX for AE and PEM, respectively. Cost reductions in the future will primarily be related to the stacks [57], and as their cost is expected to decrease faster than other categories, their cost share is expected to decrease as well. By 2030, the stacks are projected to account for 30% and 40% of the total CAPEX for AE and PEM, respectively, while in 2050, a 5% reduction in cost share is anticipated for both technologies (Table 3.9).

These economic parameters for AE and PEM in the 2030 and 2050 scenario are summarised in Table 3.9.

Table 3.9: Economic parameters for the AE and PEM in the BAU- and NZE-scenario for the years 2030 and 2050

Parameter	Unit	2030	2050	Ref.
AE				
Learning rate, LR_{AE}	%	18	10	[23] [65]
Cum. installed capacity, CAP_{AE}	GW	127	2000	[66] [67]
OPEX, $OPEX_{AE,\%}$	%	1.5	1	
PEM				
Learning rate, LR_{PEM}	%	18	10	[23] [65]
Cum. installed capacity, CAP_{PEM}	GW	63	2000	[66] [67]
OPEX, $OPEX_{PEM,\%}$	%	1.5	1	

Studies suggest that electrolysers have a similar learning rate to solar PV due to similarities in their technology structure [23]. According to a DNV study, the current learning rate for solar PV is 26%, and it's estimated to decrease to 17% by 2050 [65]. IRENA surveyed studies that estimated learning curves, and most studies reported learning curves of around 18% [23]. The Hydrogen Council predicts learning rates of 9% for AE and 13% for PEM until 2030, which are applied to both in this study [68]. Based on the average of values reported by DNV and IRENA, the current learning rate is 22%. The study implemented a learning rate of 18% for 2030 and 10% for 2050.

If all currently planned projects are realized, the total electrolyser capacity could be between 134-240 GW [66]. This study uses the median value, resulting in an estimated total installed capacity of 190 GW by 2030. However, according to the IEA, one third of the capacity will be for PEM and two thirds for AE [66]. By 2050, a 50/50 division is assumed for the installed capacity of PEM and AE technology. To reach climate goals, estimates for the installed capacity in 2050 vary between 3 TW and 5 TW [41], [67]. Therefore, this study assumes a median of 4 TW total capacity, with 2 TW of AE and 2 TW of PEM capacity.

According to Table 3.8, the OPEX is about 2.5% of the total CAPEX for AE. For PEM, the OPEX is 2% of the total CAPEX. It is assumed that for both technologies, the OPEX will decrease to 1.5% by 2030, and to 1% by 2050.

3.5.3. Vanadium redox flow battery

According to the European Association for Storage of Energy (EASE), the CAPEX for flow batteries lies between 100-400 €/kWh. Therefore it is assumed that the starting point CAPEX is 250 €/kWh. Another 25% cost reduction is assumed, which is the average of the cost reductions that the electrolysers experience, because of a direct coupling with a wind turbine. This results in a CAPEX of 190 €/kWh for the VRFB. It is likely that the capacity of the VRFB is significantly smaller than the electrolyser system, since it operates as back-up storage. Since the OPEX of the VRFB is only a couple percent of its CAPEX, the OPEX are considered negligible.

The economic parameters for the 2030 and 2050 scenario are presented in Table 3.10

Table 3.10: Economic parameters for the wind turbine for the years 2030 and 2050

Parameter	**Unit**	**2030**	**2050**	
Learning rate, LR_{fb}	%	13	10	[69]
Cum. installed capacity, CAP_{fb}	GW	3	160	[69]

In a most recent study by Louwen & Junginger (2021), the learning rate VRFBs is 13% with an error margin of 3 % [69]. In this study it is assumed that the learning rate for VRFBs will be 13 % until 2030. For the 2050 scenario it is assumed that the learning rate will drop to 10 %, assuming that VRFB's reached maturity by then.

It is expected that the flow battery capacity will reach 3 GW by 2030 [70]. In a progressive case, the installed capacity for flow batteries will reach 160 GW by 2050 [69].

4

Results

This section provides the results of the study, covering the wind turbine output in Section 4.1, sizing results for various system configurations in Section 4.2, and future cost projections of individual components in Section 4.3, based on the cost analysis presented in Section 3.5. Section 4.4 explores the systems' performance in terms of hydrogen production, while Section 4.5 presents the LCOH results. Finally, we conduct a sensitivity analysis in Section 4.6 to analyze the impact of various cost components.

4.1.Wind turbine output

Section 3.3 analyzed the past ten years of wind data for system sizing and created a distribution of time periods below the cut-in wind speed. The energy produced by the wind turbine was calculated for each year, and 2020 was chosen as the representative year due to its similarity to the average. The wind turbine produced 85 GWh of energy in 2020, resulting in a capacity factor of nearly 65% for a 15MW reference turbine. The wind turbine's duration curve is shown in Figure 4.1.

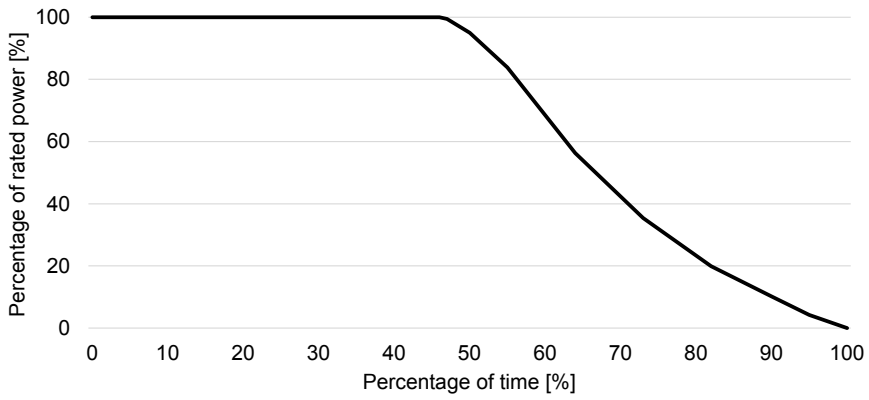

Figure 4.1: The characteristic output of the 15 MW reference turbine for the year 2020, based on KNMI data at the location of the offshore platform A12CPP

4.2.Sizing results

Figure 4.1 shows the sizing results for the system configurations analyzed in this study. Capacities for the electrolyser, battolyser, and VRFB are rounded to the nearest half value. All configurations assume a wind turbine auxiliary power demand of 100 kW and an auxiliary energy demand of 4.3 kW, based on a Δt_{max} of 43 hours. The remaining auxiliary power and energy demand is provided by the electrolyser, for which Δt_{sb} = 2. In Section 3.3, it was assumed that the maximum allowable electrolyser shutdowns throughout its lifetime is 2500.

Using Δt_{sb} = 2 resulted in 2349 shutdowns.

In the electrolyser-battolyser configuration, it was determined that a maximum electrolyser capacity of 11 MW could be installed. This allows for a 4 MW/MWh battolyser to be installed, which can supply the maximum power and energy demand while accounting for increased saturation capacity (1.45 times nominal capacity) and efficiency. The battolyser is assumed to operate at a maximum charge rate of 1C. The contribution of the electrolyser to the maximum auxiliary power and energy demand is 0.2 MW and 0.4 MWh, respectively.

In the electrolyser-VRFB configuration, a maximum electrolyser capacity of 14.5 MW can be installed. Accounting for the VRFB efficiency, a 0.5/6 MW/MWh VRFB is the minimum capacity required to meet the power and energy demand. The contribution of the electrolyser to the maximum power and energy demand in this configuration is 0.3 MW and 0.6 MWh, respectively.

For the battolyser-only scenario, the battolyser of 15 MW is installed, equal to the wind turbine capacity. In this case, the auxiliary energy and power demand is related to the wind turbine only.

Table 4.1: System sizing results of the possible system configurations an the maximum auxiliary energy and power demand per system configuration

Parameter	Unit	Value
Electrolyser-battolyser configuration		
Electrolyser capacity	MW	11
Battolyser capacity	MW/MWh	4/4
Max. auxiliary energy demand	MWh	4.7
Max. auxiliary power demand	MW	0.3
Electrolyser-VRFB configuration		
Electrolyser capacity	MW	14.5
Total battery capacity	MW/MWh	0.5/6
Max. auxiliary energy demand	MWh	4.9
Max. auxiliary power demand	MW	0.4
Battolyser-only configuration		
Battolyser capacity	MW/MWh	15/15
Max. auxiliary energy demand	MWh	4.3
Max. auxiliary power demand	MW	0.1

Annual auxiliary energy demand

Figures 4.2 and 4.3 display the annual auxiliary energy demand of the wind turbine and electrolyser for 2030 and 2050, respectively. The results are based on wind data from the year 2020 to allow for analysis of the annual auxiliary energy demand.

In the 2030 scenario, the electrolyser-VRFB systems, AEV and PEMV, exhibit higher energy demand compared to the AEB and PEMB system. Additionally, the systems involving a PEM

battolyser demonstrate lower energy demand compared to the systems involving an alkaline electrolyser. The AEV system has the highest annual auxiliary energy demand of 108 MWh, with respective shares of 62% and 38% for the electrolyser and wind turbine. The PEMB system has the lowest auxiliary energy demand with 81 MWh per year, with shares of 49% and 51% for the auxiliary electrolyser and wind turbine demand, respectively. The wind turbine's auxiliary energy demand is consistent across all systems and has a value of 41 MWh.

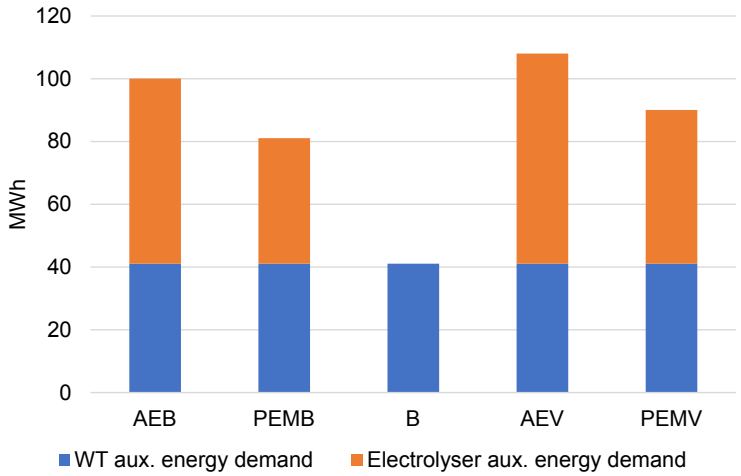

Figure 4.2: Annual auxiliary energy demand of the systems in the 2030 scenario

In the 2050 scenario, the auxiliary energy demand for systems involving AE and PEM are equal per configuration. The electrolyser-VRFB configuration still has the highest energy demand with 90 MWh. The electrolyser and wind turbine's auxiliary energy demand comprise 54% and 46% of the total, respectively. The electrolyser-battolyser configurations both have an energy demand of 81 MWh, with shares of 51% and 49% for the auxiliary electrolyser and wind turbine demand, respectively.

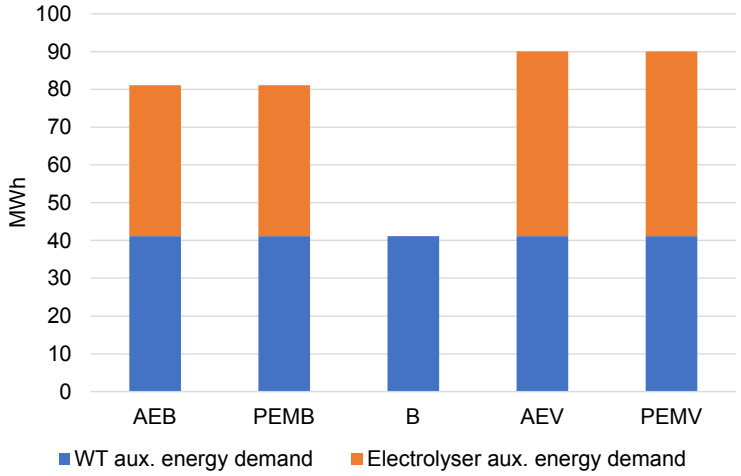

Figure 4.3: Annual auxiliary energy demand of the systems in the 2050 scenario

Based on Figure 4.2 and 4.3, the auxiliary energy demand represents approximately 0.1% of the total annual energy production of the wind turbine for the representative year 2020, which was 85 GWh.

4.3.Future cost projections

In this section the future cost projections of the system components are presented based on the economic parameters presented in Section 3.5.

Wind turbine

Based on the system design in this study, the current wind turbine capital expenditure (CAPEX) was assumed to be 2160 €/kW. By 2030, assuming a learning rate of 10% and a cumulative installed fixed-bottom offshore wind capacity of 250 GW, the wind turbine's estimated CAPEX is expected to reduce to 1770 €/kW, as shown in Figure 4.4. For the 2050 scenario, a learning rate of 5% and an installed capacity of 1100 GW were assumed, resulting in a projected CAPEX of 1580 €/kW by 2050. The reduction in CAPEX by 2030 relative to the current estimate is 18%, and by 2050, the wind turbine's CAPEX will decrease by 27%. The reduction in CAPEX by 2050 relative to 2030 is 12%.

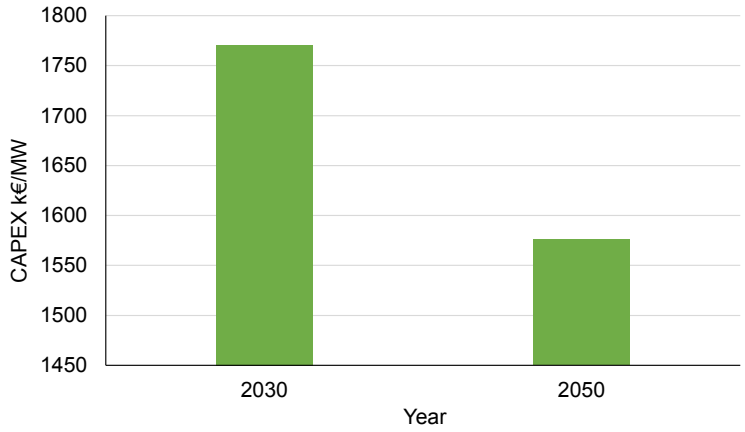

Figure 4.4: Future CAPEX projections of the wind turbine in 2030 and 2050.

Electrolysers

Figure 4.5 shows the estimated future CAPEX for AE and PEM. The starting point CAPEX for AE is 650 €/kW. Based on a learning rate of 18% and a cumulative installed capacity of 127 GW in 2030, the AE CAPEX is expected to reach 148 €/kW by 2030. For 2050, a learning rate of 10% is assumed, and the installed capacity is estimated to reach 2000 GW, resulting in a projected CAPEX of 98 €/kW. Relative to the current CAPEX estimate, the CAPEX reduction by 2030 is 77%. By 2050, the AE CAPEX will be reduced by 85%. The reduction in CAPEX by 2050 relative to 2030 is 34%.

The starting point CAPEX for PEM is 765 €/kW. Based on a learning rate of 18% and a cumulative installed capacity of 63 GW in 2030, the PEM CAPEX is expected to reach 175 €/kW by 2030. For 2050, a learning rate of 10% is assumed, and the installed capacity is estimated to reach 2000 GW, resulting in a projected CAPEX of 104 €/kW. Relative to the current CAPEX estimate, the CAPEX reduction by 2030 is 77%. By 2050, the PEM CAPEX will be reduced by 87%. The reduction in CAPEX by 2050 relative to 2030 is 44%.

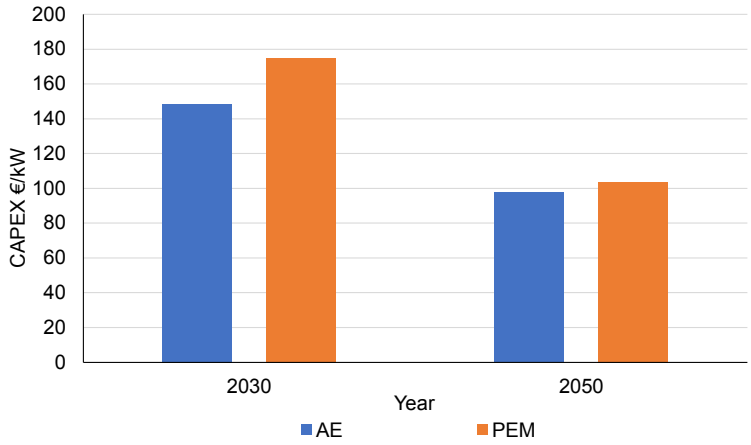

Figure 4.5: Future CAPEX projections for AE and PEM in 2030 and 2050

VRFB

Figure 4.5 presents the estimated future CAPEX for the VRFB. The starting point CAPEX for the VRFB is 190 €/kWh. Based on a learning rate of 13% and a cumulative installed capacity of 3 GW in 2030, the VRFB CAPEX is expected to reach 140 €/kWh by 2030. For 2050, a learning rate of 10% is assumed, and the installed capacity is estimated to reach 160 GW, resulting in a projected CAPEX of 81 €/kWh. Relative to the current CAPEX estimate, the CAPEX reduction by 2030 is 26%. By 2050, the VRFB CAPEX will be reduced by 57%. The reduction in CAPEX by 2050 relative to 2030 is 42%.

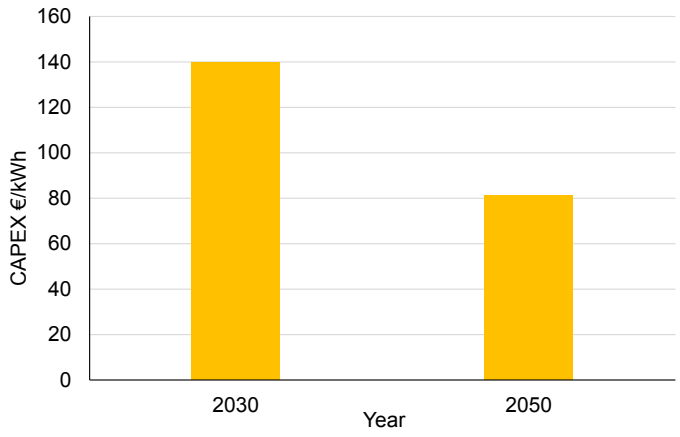

Figure 4.6: Future CAPEX projections of the VRFB in 2030 and 2050.

4.4.System performance

This section presents the performance of different systems. In the 2030 scenario, the B system produced the most hydrogen (1572 tonnes) while the PEMV system produced the least. The electrolyser contributed 80% of hydrogen production in both AEB and PEMB systems, with the battolyser making up the remaining 20%. In the 2050 scenario, the B system also produced the highest amount of hydrogen (1652 tonnes) while the AEV system produced the least.

Like in the 2030 scenario, the electrolyser was responsible for 80% of hydrogen production in both AEB and PEMB systems, with the battolyser contributing the remaining 20%. Lastly, the percentage of H_2 energy content relative to the total energy produced by the wind turbine for each system in 2030 and 2050 is shown.

Table 4.2: Performance of the various systems in terms of hydrogen output for the years 2030 and 2050

Parameter	**Unit**	**AEB**	**PEMB**	**B**	**AEV**	**PEMV**
2030						
Total production	**tonnes**	**1559**	**1494**	**1572**	**1507**	**1438**
% produced by electrolyser	%	80	79	-	100	100
% produced by battolyser	%	20	21	100	-	-
H_2 energy content as % of total WT energy produced	%	72	69	73	70	67
2050						
Total production	**tonnes**	**1642**	**1655**	**1658**	**1611**	**1616**
% produced by electrolyser	%	80	80	-	100	100
% produced by battolyser	%	20	20	100	-	-
H_2 energy content as % of total WT energy produced	%	77	77	77	75	75

4.5.LCOH results

This section presents the LCOH of different systems for the 2030 and 2050 scenarios. The LCOH for each system is plotted against various battolyser CAPEX values to determine which system is most cost-effective at different CAPEX values. First, the electrolyser-battolyser and electrolyser-VRFB configurations are compared for both scenarios. Then, the electrolyser-battolyser and battolyser-only configurations are compared. Finally, a waterfall chart is included to break down the LCOH for a specific system and battolyser price, providing an overview of how the LCOH of an offshore-hydrogen system is calculated.

Figure 4.7 compares the AEB, PEMB, AEV, and PEMV systems for the 2030 scenario. The LCOH of the AEV and PEMV systems remains constant, as they do not include a battolyser. The LCOH of the AEV and PEMV systems are 1.55 €/kg and 1.67 €/kg, respectively. The systems with PEM electrolysers are more costly than the systems with an alkaline electrolyser. The AEV system is the preferred option in terms of LCOH for a battolyser CAPEX > 390 €/kW, while the AEB system is the preferred option for a battolyser CAPEX < 390 €/kW.

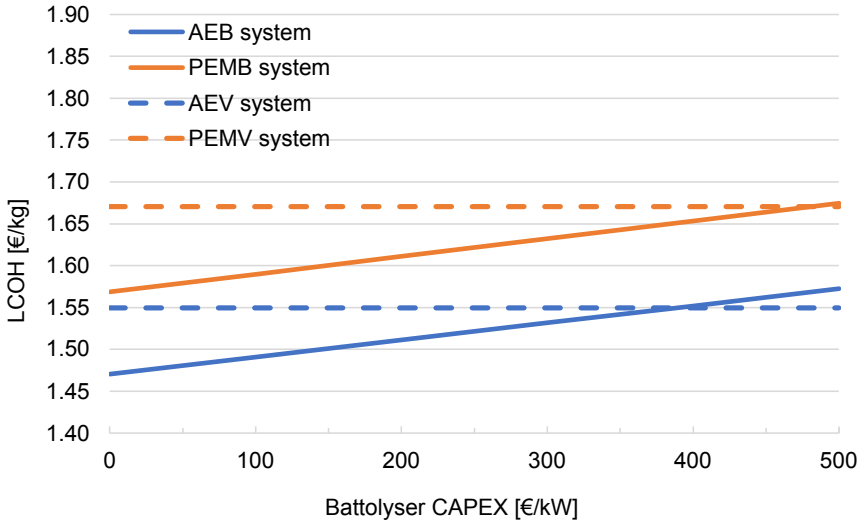

Figure 4.7: LCOH of the electrolyser-battolyser and electrolyser-VRFB configurations in 2030, as a function of the battolyser CAPEX

Figure 4.8 compares the same systems as in the 2030 scenario, but for 2050. The LCOH of the AEV and PEMV systems are approximately the same, at 1.18 €/kg. The difference in LCOH between the AEB and PEMB systems is minimal as well. The preferred systems in terms of LCOH for a battolyser CAPEX > 250 €/kW are the AEV and PEMV systems, while the AEB and PEMB systems are the preferred options for a battolyser CAPEX < 250 €/kW.

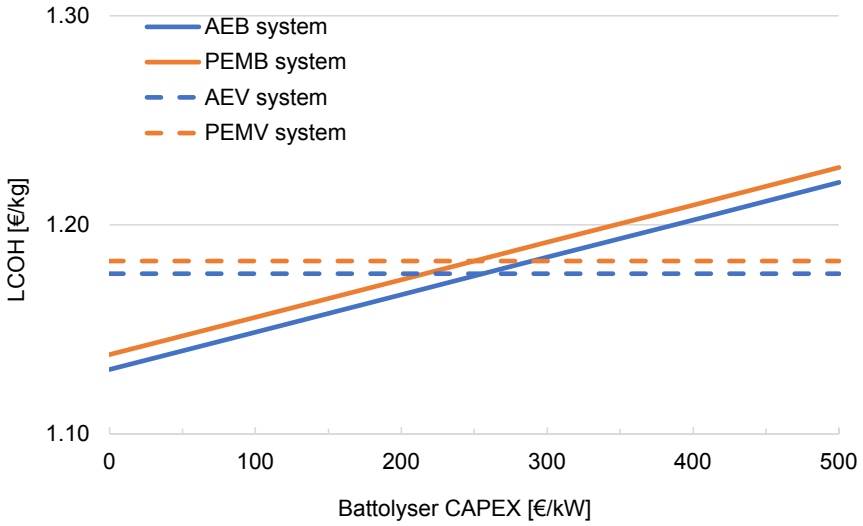

Figure 4.8: LCOH of the electrolyser-battolyser and electrolyser-VRFB configurations in 2050, as a function of the battolyser CAPEX

Figures 4.9 and 4.10 compare the LCOH results of the electrolyser-battolyser and battolyser-only configurations for the 2030 and 2050 scenarios. In both cases, the B system exhibits a steeper rise in LCOH for higher battolyser CAPEX due to its larger battolyser capacity. In the 2030 scenario, the AEB system is the most cost-effective choice for CAPEX values above 175 €/kW. The B system yields a lower LCOH for CAPEX values below 175 €/kW.

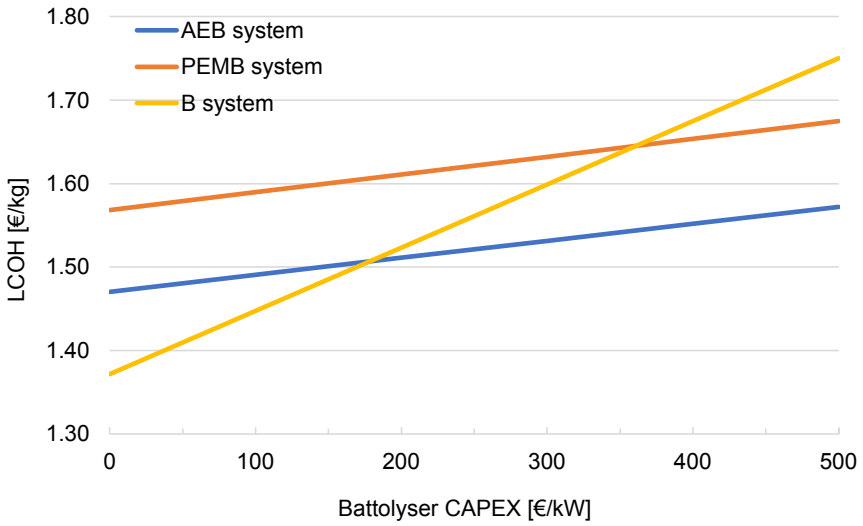

Figure 4.9: LCOH of the electrolyser-battolyser and battolyser-only configurations in 2030, as a function of the battolyser CAPEX

In the 2050 scenario, the AEB and PEMB systems are the desired systems in terms of LCOH for a battolyser CAPEX > 120 €/kW. For a CAPEX < 120 €/kW, the battolyser is the desired system.

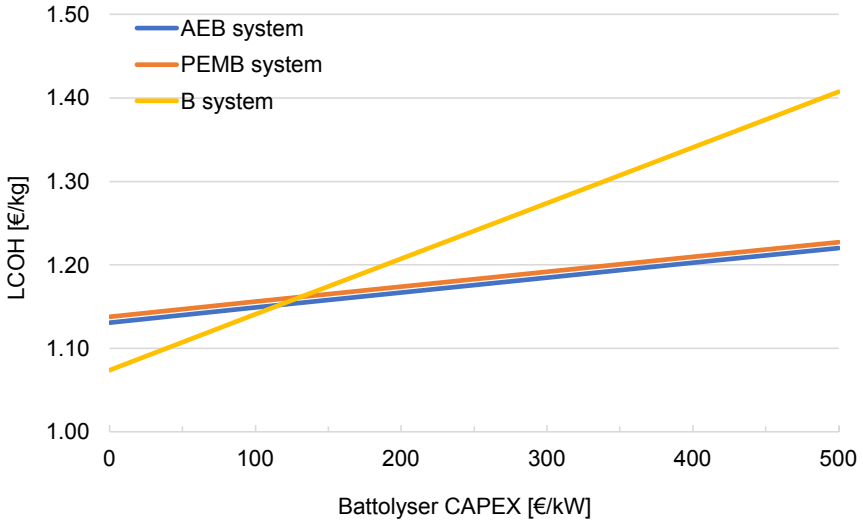

Figure 4.10: LCOH of the electrolyser-battolyser and battolyser-only configurations in 2050, as a function of the battolyser CAPEX

To provide a general understanding of how the LCOH of an offshore wind-hydrogen system is calculated, the AEB system is used as an example with a fixed battolyser CAPEX of 200 €/kW for both the 2030 and 2050 scenarios. Waterfall charts are shown in Figures 4.11 and 4.12 to display the breakdown of LCOH per cost component. The wind turbine component contributes the most to the LCOH, followed by the alkaline electrolyser CAPEX. This pattern holds true for both scenarios. For this particular AEB system, the LCOH is 1.51 €/kg in the 2030 scenario.

Figure 4.11: LCOH breakdown of an AEB system for a battolyser CAPEX of 200 €/kW in the 2030 scenario.

Despite the various rates at which costs per component decline, the contributions per cost components stay about the same. The LCOH of this specific system in 2050 is 1.15 €/kg.

Figure 4.12: LCOH breakdown of an AEB system for a battolyser CAPEX of 200 €/kW in the 2050 scenario.

For the sensitivity analyses, the same AEB system is analysed, again with a battolyser CAPEX of 200 €/kW.

4.6.Sensitivity analysis

In Figures 4.13 and 4.14, the sensitivity analyses are presented for the years 2030 and 2050. The same AEB system is analysed, again with a battolyser CAPEX of 200 €/kW. The minimum and maximum values for the LCOH are caused by CAPEX variations of the wind turbine. In 2030, the minimum value is 0.8 €/kW and the maximum value is 2.2 €/kW. The second largest driver is the WACC, yielding values for the LCOH of 1.1-2.0 €/kW.

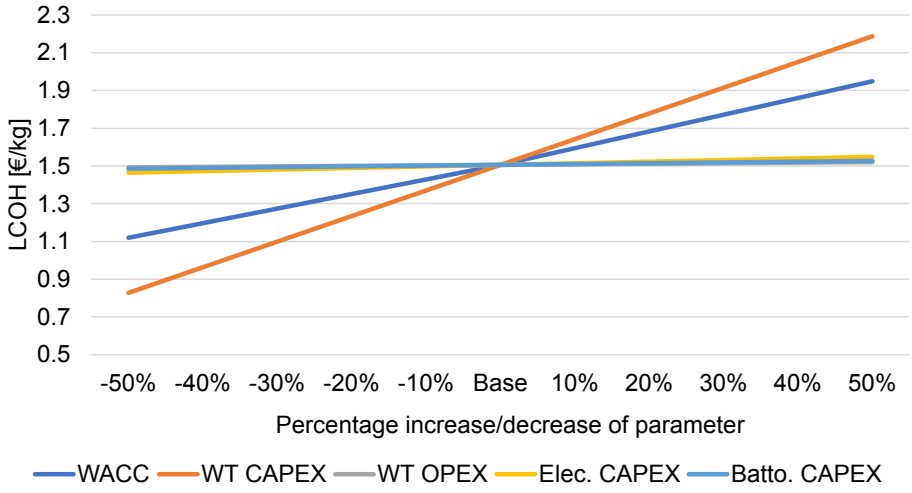

Figure 4.13: LCOH the AE- PB- and B-system in 2030, for a range of values for the battolyser CAPEX

In 2050, the minimum value is about 0.6 €/kW and the maximum value is 1.7 €/kW. The WACC yields a value of about 0.8 €/kW in 2030, and a value of just over 1.5 €/kW by 2050.

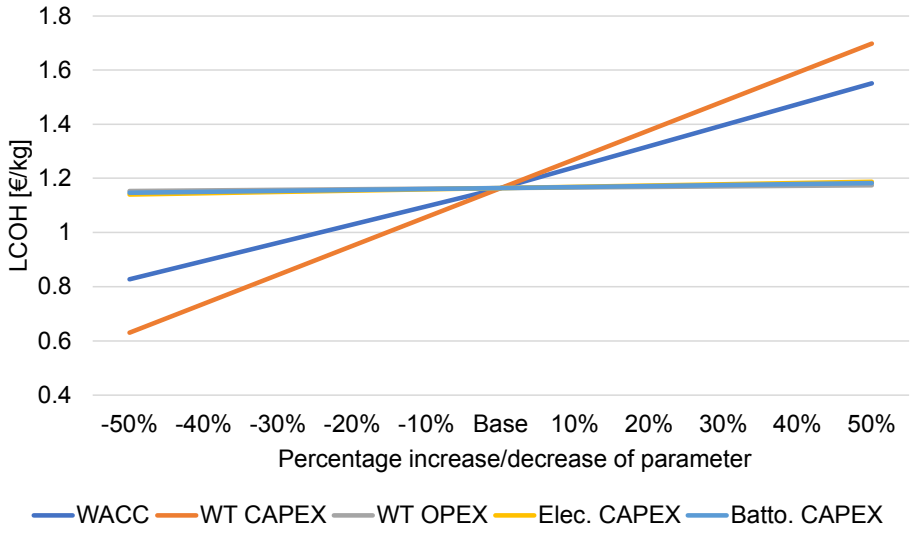

Figure 4.14: LCOH the AE- PB- and B-system in 2030, for a range of values for the battolyser CAPEX

Finally, the LCOH was calculated for the system if the wind turbine and other components were not directly connected via the DC-link. In the 2030 scenario, this would result in a LCOH of 1.53 €/kW, which is 1.3% higher than the direct connection with the wind turbine. In the 2050 scenario, this would result in a LCOH of 1.17 €/kW, which is 0.9% higher than the directly connected system.

5

Discussion

In this section, first a short paragraph with key findings is presented. Then the results will be interpreted in the sequential order as stated in Section 4. Thereafter, the limitations of this researched will be discussed.

Results interpretation

The objective of this study was to investigate the techno-economic feasibility and viability of an offshore wind-hydrogen system incorporating battolyser technology. The study analyzed the system for the years 2030 and 2050, considering that battolyser technology is still in its infancy. Results indicate that a system incorporating battolyser technology outperforms a system with a VRFB in terms of hydrogen production. The LCOH of a system incorporating battolyser technology could fall below 1.5 €/kg by 2030 and even below 1.2 €/kg by 2050, based on battolyser CAPEX. The wind turbine is identified as the primary cost driver, accounting for over 85% of the total LCOH for both scenarios. Therefore, variations in other system components' costs have a negligible effect on the LCOH of the system, as demonstrated in the sensitivity analyses.

The sizing of the system is determined by the auxiliary power and energy demand of the wind turbine and electrolyser. The maximum auxiliary energy demand of the wind turbine is constant across all cases, so any variation in the total maximum auxiliary energy demand is dependent on the standby time of the electrolyser. The standby time of the electrolyser is determined by the maximum allowable number of shutdowns, which is assumed to be 2500 in this study (as presented in Section 3.3). Allowing a higher number of shutdowns would decrease the necessary storage capacity, leading to an increased electrolyser capacity. However, data on the relationship between the number of shutdowns and the system's lifetime is limited. In this study, it is assumed that exceeding the number of shutdowns reduces the electrolyser's lifetime. It would be valuable to have more precise information on the exact decrease in lifetime for a given number of shutdowns. Combining this information with the additional cost of maintaining an electrolyser in hot standby would provide valuable insights for determining the appropriate control strategy.

In Section 4.2, the annual auxiliary energy demand values were presented. The electrolyser-VRFB configurations had a higher energy demand because of the larger size of the electrolyser, which results in a higher auxiliary energy demand. In the 2030 scenario, systems with a PEM electrolyser had a lower auxiliary energy demand compared to alkaline electrolyser systems. This was because the alkaline electrolyser has a higher minimum operational load, which means that it is shut down for a more extended period than the PEM electrolyser. By 2050, the auxiliary energy demand of a system with a PEM electrolyser will be equivalent to an alkaline electrolyser system. This is because the electrolyser technologies' performance is assumed to converge over time and have the same technical parameters by 2050. As previously mentioned, the wind turbine produced 85 GWh of total energy in 2020, and the auxiliary energy demand

is insignificant when compared to the annual energy produced by the wind turbine. However, satisfying the auxiliary energy demand is necessary for the operation of an autonomous offshore system.

It has been observed that the offshore wind-hydrogen system will be most expensive due to the wind turbine component in both the years of 2030 and 2050. The cost of the wind turbine is anticipated to decrease at a slower rate compared to other components. This is due to the fact that wind turbines are complex machines, and as such, they have a low learning rate for cost reduction. Additionally, their technology is already established, which limits opportunities for disruptive innovation that could drive down costs.

The electrolysers, on the other hand, are projected to decrease in cost faster than the wind turbine, with an average cost reduction of 40% from 2030 to 2050. Electrolysers are a newer and less complex technology, with considerable potential for innovation and cost reduction compared to wind turbines. As the electrolyser market is still in development, there is ample opportunity for efficiency and cost improvements, leading to a higher learning rate as production scales up. The market share for PEM is expected to increase due to its flexibility and the growing installed renewable energy capacity. However, it remains to be seen whether AE or PEM technology will dominate, as both are capable of following the load fluctuations of wind and solar, according to IRENA [23].

The capital expenditures (CAPEX) of the vanadium redox flow batteries (VRFB) are estimated to have a learning rate of 13% in 2030 and 10% in 2050. However, according to Junginger et al., VRFBs are at the brink of commercialization [69]. In the future, VRFBs have the potential to be a revolutionary technology for long-term stationary storage. The installed capacity and technological improvements in VRFBs may result in a higher learning rate, which could reduce the CAPEX of VRFBs.

Upon analyzing the performance of the systems in Table 4.2, it can be observed that in the 2030 scenario, systems incorporating an alkaline electrolyser produce more hydrogen compared to those incorporating a PEM electrolyser. This difference can be explained by comparing the technical parameters of the two assets in Table 3.3. In 2030, the DC efficiency of AE is higher, and the stack degradation is lower than that of PEM. Although PEM is more efficient at partial loads, AE produces more hydrogen. However, in 2050, the technical parameters for both technologies are similar, and it can be observed that PEM produces slightly more hydrogen than AE because it operates at higher efficiencies at lower loads.

The systems incorporating a battolyser exhibit higher hydrogen production due to their larger electrolysis capacity, as demonstrated by the system sizing results presented in Table 4.2. This trend persists in both 2030 and 2050 as the sizing remains constant. The B system performs the best in terms of hydrogen production in both scenarios, likely due to its higher partial load characteristics. This is because the technical parameters for AE, PEM, and the battolyser are almost identical in 2050. Although the minimum load for the battolyser is lower, the extra hydrogen production resulting from this feature is likely negligible.

The systems incorporating a PEM electrolyser exhibit the highest CAPEX in terms of LCOH for both the 2030 and 2050 scenarios. This is because, in the 2030 scenario, PEM systems produce less hydrogen and are more expensive compared to other technologies. In the 2050 scenario, although the hydrogen yield for PEM is slightly higher, the associated cost is also slightly higher, resulting in a LCOH that is higher than that of a system incorporating AE technology in 2050.

The LCOH of the AEV and PEMV systems are expected to reach 1.55 and 1.67 €/kg, respec-

tively, in 2030, as indicated by Figure 4.7. The absence of a battolyser in the electrolyser-VRFB systems in Section 4.5 is evident from the horizontal LCOH graphs. For a battolyser CAPEX of 400 €/kg or higher, the AEV system is the preferred choice, as the AEB system does not produce enough hydrogen to offset the battolyser CAPEX, making it less competitive than the AEV system. However, for a battolyser price below 400 €/kg, the AEB system is the most cost-effective option, with a maximum LCOH of 1.55 €/kg. Considering the synergy between AE technology and battolyser technology, it is anticipated that the battolyser CAPEX will eventually catch up with the CAPEX of established technologies. Therefore, a battolyser CAPEX of 200 €/kg is achievable and would be slightly higher than the CAPEX for PEM, yielding an LCOH of about 1.5 €/kg for the AEB system. With an LCOH of 1.5 €/kg, hydrogen could become a practical alternative to fossil fuels, particularly in industries such as heavy industry and transportation, where alternatives to fossil fuels are limited. For the B system, it becomes cost-competitive with the AEB system for a battolyser CAPEX of approximately 175 €/kg, as presented in Figure 4.9. Assuming a battolyser price of 200 €/kg, the AEB system would still be the most cost-effective choice.

In 2050, the LCOH of the AEV and PEMV systems are almost identical, at around 1.18 €/kg. Similarly, the difference between the AEB and PEMB systems is negligible. For a battolyser price below 250 €/kg, an electrolyser-battolyser configuration is the most cost-effective option. By 2050, the battolyser CAPEX is expected to catch up with established technologies, resulting in a battolyser CAPEX of 100 €/kg, according to Figure 4.5. For a CAPEX of 100 €/kg, the electrolyser-battolyser configurations are the preferred systems, with an LCOH of approximately 1.15 €/kg. At an LCOH of 1.15 €/kg, the electrolyser-battolyser systems become cost-competitive with blue hydrogen and green hydrogen produced by solar energy, as presented in scenarios by McKinsey & Company [71]. Although the B system yields a slightly lower LCOH, the general trend towards 2050 is that the LCOH of various systems converges, and the impact of changing the battolyser price becomes smaller.

The waterfall charts in Figures 4.11 and 4.12 indicate that the wind turbine is the largest cost contributor in the system. In an AEB system with a battolyser CAPEX of 200 €/kg in the 2030 scenario, the wind turbine's LCOH contribution is 1.33 €/kg, accounting for 89% of the total LCOH. This demonstrates that a reduction in the electrolyser or battolyser CAPEX does not have a significant impact on cost reduction. Conversely, reducing the wind turbine cost would result in a significant reduction in costs. The wind turbine's cost reduction rate is the lowest among the system components, which means that in 2050, the wind turbine's LCOH share is just over 90%. Therefore, the same conclusion applies to the 2050 scenario.

Figures 4.13 and 4.14 illustrate how changing various cost parameters affects the LCOH. The results are presented for an AEB system with a battolyser CAPEX of 200 €/kg. As anticipated, the wind turbine has the greatest impact on the LCOH. In both the 2030 and 2050 scenarios, a 20% and 50% reduction in the wind turbine cost makes the system less expensive than the most optimistic green hydrogen scenario presented by McKinsey & Company [71].

At the end of the sensitivity analysis, the results were presented for an AEB system with a battolyser CAPEX of 200 €/kW, assuming it was not directly connected to the wind turbine. The findings revealed a 1.3% increase in LCOH for 2030 and a 0.9% increase for 2050. The analysis assumed that the electrolysis could still take place in or at the turbine, but the power conversion system of the electrolyser was considered. The primary benefit, therefore, is improved efficiency rather than cost savings on conversion equipment.

Research limitations

It is assumed that the Dutch Exclusive Economic Zone (EEZ) will permit offshore wind installations in the Dogger Bank by 2030. However, the Dogger Bank is also a Natura 2000 area, and it is uncertain whether it will be possible to establish these installations by 2030. This will depend on various factors, such as the demand for renewable energy production at that specific location and the environmental impact it may have.

The wind speed analysis relies on hourly data gathered from offshore platforms situated near the Dogger Bank. As the wind speeds are measured and rounded to m/s units, the resulting data is relatively discrete. This aspect has an impact on the system's sizing, the quantity of hydrogen produced, and the required number of electrolyser shutdowns. Consequently, more detailed wind speed data would yield more precise outcomes.

During the system sizing process, it is assumed that both the battolyser and VRFB can discharge over a maximum period of Δt_{max}. However, this implies that the battolyser and battery can discharge continuously for up to 43 hours. While some manufacturers of VRFBs, such as CellCube, report discharge periods of up to 24 hours, this still falls short of the assumed discharge period in the system sizing process [72]. To address this issue, it may be necessary to use multiple batteries or battolysers to provide the auxiliary systems with power over Δt_{max}. However, for the sake of simplicity, the hydrogen production model does not consider minimum discharge rates, and only a single asset is modeled for every model component.

It is important to consider the impact of variable charge and discharge rates on the roundtrip efficiency of the battolyser and VRFB, as this could affect the sizing and design of offshore wind hydrogen systems. However, this phenomenon is not taken into account in this study.

In reality, the efficiency of the battolyser and VRFB can vary depending on the charge and discharge rates. Higher charge and discharge rates can lead to lower efficiency, which could have an impact on the overall performance of the offshore wind hydrogen system. Therefore, it is important to consider these factors during the sizing and design of the system.

This study provides a comprehensive overview of various system designs for offshore wind hydrogen systems, with the aim of determining whether a battolyser should be incorporated into the system. However, the study does not delve into system optimization strategies. In future studies, where a specific system is selected for a specific purpose, optimizing strategies should be researched to minimize the production cost for that purpose.

One example of economic modeling could be reducing the size of the hydrogen production system by considering the fact that wind turbines are not always operated at full load. This would depend on the amount of CAPEX that can be saved and the amount of hydrogen production that is missed out on. By conducting such optimization studies, it can ensured that the offshore wind hydrogen system is cost-effective and efficient for its intended purpose.

In addition to optimizing the offshore wind hydrogen system for production cost, it is also essential to consider the specific purpose of the system and the operational strategy required to achieve it. For instance, if the system is designed for a consistent hydrogen output, the electrolyser or battolyser must operate at a higher minimum partial load, which would require additional storage capacity depending on the reliability of the supply required.

Since this study focuses on the dynamic operation of the system and models its efficiency accordingly, it would be fascinating to explore the possibility of operating multiple electrolysers or battolysers at a smaller load. However, the feasibility of this approach would depend on the intended purpose of the system.

Overall, optimizing the offshore wind hydrogen system requires a thorough understanding of the specific purpose of the system, the operational strategy required to achieve it, and the dynamic behavior of the system. By considering these factors, we can design a cost-effective and efficient offshore wind hydrogen system that meets the intended purpose.

6

Conclusion and recommendations

This study aimed to investigate the technical and economic feasibility of a stand-alone offshore wind-hydrogen production system with battolyser technology on the Dogger Bank in 2030 and 2050. To achieve this, a literature review was conducted to gain knowledge about the Dogger Bank, system components, and structural feasibility. The hydrogen production model, developed in this study, reflects the performance of proposed system designs, taking into account dynamic operation. Using historic data, future cost projections of the model components were made. Combining the results from the hydrogen production model and future cost projections, the levelised cost of hydrogen (LCOH) of the proposed systems were analysed for the years 2030 and 2050. The following conclusions could be drawn to address the main research question as well as the sub-questions:

The analysis shows that the system is technically feasible, as the system sizing criteria are met for the various system configurations, enabling autonomous operation. Additionally, the economic feasibility is demonstrated by the LCOH results, which indicate that a system with battolyser technology can achieve competitive hydrogen production costs with a LCOH below 1.5 €/kg by 2030 and below 1.2 €/kg by 2050. The importance of the battolyser lies in its ability to enhance the system's performance in terms of hydrogen production, as well as providing the auxiliary energy supply.

A total of three system configurations have been identified, which include an electrolyser-battolyser configuration, an electrolyser-vanadium redox flow battery (VRFB) configuration, and a battolyser-only configuration. These configurations can be further divided into five specific systems: the alkaline electrolyser-battolyser (AEB) system, the PEM-battolyser (PEMB) system, the battolyser-only (B) system, the alkaline electrolyser-VRFB (AEV) system, and the PEM-VRFB (PEMV) system. In each of these systems, either the battolyser or VRFB is responsible for providing the necessary auxiliary energy supply. None of the models considered a desalination unit, as its cost and energy consumption were regarded as insignificant.

A single-factor learning curve method was used to estimate future costs for the different components of the model. The wind turbine is expected to have a capital expenditure (CAPEX) of 1770 €/kg by 2030 and 1580 €/kg by 2050. The alkaline electrolyser is predicted to have a CAPEX of 148 €/kg by 2030 and 98 €/kg by 2050. The proton exchange membrane (PEM) system is anticipated to have a CAPEX of 175 €/kg in 2030 and 104 €/kg in 2050. Finally, the VRFB is forecasted to have a CAPEX of 190 €/kg by 2030 and 81 €/kg by 2050.

The hydrogen production model utilizes future technical parameters of the system components and considers the dynamic operation of the system to calculate the hydrogen production. In both the 2030 and 2050 scenarios, the majority of hydrogen is produced by the battolyser-only (B) system. Specifically, in the 2030 scenario, the B system produces 1572 tonnes of hydrogen, followed by the AEB system with 1559 tonnes. The PEMV system produces the least amount of hydrogen in 2030. In the 2050 scenario, the B system produces 1658 tonnes of hydrogen,

followed by the PEMB system with 1655 tonnes.

The acceptable cost range for the battolyser depends on the electrolyser-VRFB configurations. Analysis revealed that in 2030, the acceptable battolyser CAPEX range is less than 400 €/kW. If the battolyser CAPEX is below 400 €/kW, all systems that include a battolyser will have a lower LCOH compared to the electrolyser-VRFB configurations. At a CAPEX of 400 €/kW, the AEB and AEV systems produce an LCOH of 1.55 €/kg. In 2050, the acceptable battolyser CAPEX range is less than 250 €/kW. At a CAPEX of 250 €/kW, all systems produce an LCOH of approximately 1.18 €/kg.

The wind turbine cost is the most crucial parameter, as it represents almost 90% of the total CAPEX in both 2030 and 2050. If the wind turbine CAPEX has a sensitivity of 50%, the LCOH range will be 0.8-2.2 €/kg in 2030. By 2050, this range decreases to 0.6-1.7 €/kg.

The first key recommendation for future studies is to focus on reducing the cost of the wind turbine. As the largest cost driver, the wind turbine has a significant impact on the levelized cost of hydrogen (LCOH). Therefore, reducing the cost of the wind turbine would be the most effective way to bring down the LCOH.

The second recommendation is to explore various operational strategies. In this study, only a single wind turbine was modeled, but modeling the hydrogen output for an entire wind farm for a specific purpose might require different operational regimes. Therefore, it would be beneficial to research various operational strategies that can optimize the performance of the offshore wind hydrogen system.

Moreover, there is a need for more detailed research into the dynamic modeling of a battolyser system combined with offshore wind. Analyzing the dynamic operations on a shorter time frame would provide more detailed insights into the dynamic performance of the battolyser combined with wind energy. This would enable us to identify any operational challenges and opportunities to improve the efficiency and effectiveness of the system.

By addressing these key recommendations, future studies can help to optimize the performance of offshore wind hydrogen systems, reduce production costs, and increase the viability of this promising technology.

References

[1] European Commission, *Offshore renewable energy*, 2022. [Online]. Available: https://energy.ec.europa.eu/topics/renewable-energy/offshore-renewable-energy_en.

[2] IEA, *Hydrogen – Analysis - IEA*, 2022. [Online]. Available: https://www.iea.org/reports/hydrogen.

[3] A. van Wijk and C. Hellinga, "Hydrogen-the key to the energy transition," 2018.

[4] North Sea Energy, *North Sea Energy*. [Online]. Available: https://north-sea-energy.eu/nl/energieatlas/.

[5] B. Geyer, R. Weisse, P. Bisling, and J. Winterfeldt, "Climatology of North Sea wind energy derived from a model hindcast for 1958-2012," *Journal of Wind Engineering and Industrial Aerodynamics*, vol. 147, pp. 18–29, Dec. 2015, ISSN: 01676105. DOI: 10.1016/J.JWEIA.2015.09.005.

[6] S. Mulder, "Offshore Wind Capacity Dogger Bank," 2017.

[7] F. M. Mulder, B. M. H. Weninger, J. Middelkoop, F. G. B. Ooms, and H. Schreuders, "ELECTRONIC SUPPLEMENTARY INFORMATION Efficient electricity storage with the battolyser, an integrated Ni-Fe battery and electrolyser," 2016.

[8] B. Jenkins, D. Squires, J. Barton, *et al.*, "Techno-Economic Analysis of Low Carbon Hydrogen Production from Offshore Wind Using Battolyser Technology," *Energies 2022, Vol. 15, Page 5796*, vol. 15, no. 16, p. 5796, Aug. 2022, ISSN: 1996-1073. DOI: 10.3390/EN15165796. [Online]. Available: https://www.mdpi.com/1996-1073/15/16/5796/htm%20https://www.mdpi.com/1996-1073/15/16/5796.

[9] United Nations, *PREAMBLE TO THE UNITED NATIONS CONVENTION ON THE LAW OF THE SEA*, 1994. [Online]. Available: https://www.un.org/depts/los/convention_agreements/texts/unclos/part5.htm.

[10] E. L. Bravo, R. A. Van Mastrigt, K. Didderen, and S. Mulder, "Doeluitwerking Doggersbank," *Royal HaskoningDHV & Bureau Waardenburg Ecologie en Landschap - Rapport Doeluitwerking Doggersbank*, [Online]. Available: https://www.rwsnatura2000.nl/gebieden/eez/eez_documenten/handlerdownloadfiles.ashx?idnv=1415365.

[11] KNMI, *KNMI - Uurgegevens van Noordzee stations*. [Online]. Available: https://www.knmi.nl/nederland-nu/klimatologie/uurgegevens_Noordzee.

[12] Energinet, "ANALYSIS OF CONSTRAINTS IN DOGGER BANK," 2017. [Online]. Available: https://northseawindpowerhub.eu/sites/northseawindpowerhub.eu/files/media/document/Analysis-of-constraints-in-Dogger-Bank.pdf.

[13] R. Peters, J. Vaessen, and R. Van Der Meer, "Offshore hydrogen production in the north sea enables far offshore wind development," *Proceedings of the Annual Offshore Technology Conference*, vol. 2020-May, 2020, ISSN: 01603663. DOI: 10.4043/30698-MS. [Online]. Available: https://www.researchgate.net/publication/341064809_Offshore_Hydrogen_Production_in_the_North_Sea_Enables_Far_Offshore_Wind_Development.

[14] Dogger Bank Wind Farm, *Dogger Bank Wind Farm*. [Online]. Available: https://doggerbank.com/about/.

[15] Sofia Offshore Wind Farm, *Sofia Offshore Wind Farm, Dogger Bank*. [Online]. Available: https://sofiawindfarm.com/.

[16] E. Gaertner, J. Rinker, L. Sethuraman, *et al.*, "Definition of the IEA Wind 15-Megawatt Offshore Reference Wind Turbine Technical Report," 2020. [Online]. Available: www.nrel.gov/publications..

[17] COTES, "WIND TURBINES NEED PROTECTING AGAINST THE EFFECTS OF HUMIDITY COTES.COM," 2017. [Online]. Available: https://f.hubspotusercontent00.net/hubfs/7154103/On-and-offshore-Brochure_30.10.17.pdf.

[18] M. Froese, *The key role of energy storage backup power for wind-turbine pitch control*, Feb. 2018.

[19] Berggren J, "Teknisk-naturvetenskaplig fakultet UTH-enheten," 2013. [Online]. Available: http://www.teknat.uu.se/student.

[20] I. Energy Agency, "Net Zero by 2050 - A Roadmap for the Global Energy Sector," 2022. [Online]. Available: www.iea.org/t&c/.

[21] X. Zhang, S. H. Chan, H. K. Ho, *et al.*, "Towards a smart energy network: The roles of fuel/electrolysis cells and technological perspectives," *International Journal of Hydrogen Energy*, vol. 40, no. 21, pp. 6866–6919, Jun. 2015, ISSN: 0360-3199. DOI: 10.1016/J.IJHYDENE.2015.03.133.

[22] N. Gallandat, K. Romanowicz, and A. Züttel, "An Analytical Model for the Electrolyser Performance Derived from Materials Parameters," *Journal of Power and Energy Engineering*, vol. 05, no. 10, pp. 34–49, 2017, ISSN: 2327-588X. DOI: 10.4236/JPEE.2017.510003.

[23] T. International Renewable Energy Agency, "GREEN HYDROGEN COST REDUCTION SCALING UP ELECTROLYSERS TO MEET THE 1.5°C CLIMATE GOAL H 2 O 2," 2020. [Online]. Available: www.irena.org/publications.

[24] F. Mulder and H. Geerlings, *Hydrogen-electrolysis-1-2021 - SET3085 Hydrogen Technology (2020/21 Q4)*. [Online]. Available: https://brightspace.tudelft.nl/d2l/le/content/280748/viewContent/2129804/View.

[25] Dr. P. Lettenmeier (SIemens Energy), "Efficiency-Electrolysis White paper siemens-energy.com/electrolyzer," 2021. [Online]. Available: https://assets.siemens-energy.com/siemens/assets/api/uuid:a33a8c39-b694-4d91-a0b5-4d8c9464e96c/efficiency-white-paper.pdf.

[26] McKinsey & Company, *Higher heating value | McKinsey Energy Insights*. [Online]. Available: https://www.mckinseyenergyinsights.com/resources/refinery-reference-desk/higher-heating-value/.

[27] E. Frank, J. Gorre, F. Ruoss, and M. J. Friedl, "Calculation and analysis of efficiencies and annual performances of Power-to-Gas systems," *Applied Energy*, vol. 218, pp. 217–231, May 2018, ISSN: 03062619. DOI: 10.1016/J.APENERGY.2018.02.105.

[28] A. Ursúa, E. L. Barrios, J. Pascual, I. San Martín, and P. Sanchis, "Integration of commercial alkaline water electrolysers with renewable energies: Limitations and improvements," *International Journal of Hydrogen Energy*, vol. 41, no. 30, pp. 12 852–12 861, Aug. 2016, ISSN: 03603199. DOI: 10.1016/J.IJHYDENE.2016.06.071.

[29] G. Matute, J. M. Yusta, J. Beyza, and L. C. Correas, "Multi-state techno-economic model for optimal dispatch of grid connected hydrogen electrolysis systems operating under dynamic conditions," *International Journal of Hydrogen Energy*, vol. 46, no. 2, pp. 1449–1460, Jan. 2021, ISSN: 03603199. DOI: 10.1016/J.IJHYDENE.2020.10.019.

[30] F. M. Mulder, B. M. H Weninger, J. Middelkoop, F. G. B Ooms, and H. Schreuders, "Efficient electricity storage with a battolyser, an integrated Ni-Fe battery and electrolyser †," *Energy Environ. Sci*, vol. 10, p. 756, 2017. DOI: 10.1039/c6ee02923j. [Online]. Available: www.rsc.org/ees.

[31] R. K. Sankaralingam, S. Seshadri, J. Sunarso, A. I. Bhatt, and A. Kapoor, "Overview of the factors affecting the performance of vanadium redox flow batteries," *Journal of Energy Storage*, vol. 41, Sep. 2021, ISSN: 2352152X. DOI: 10.1016/J.EST.2021.102857.

[32] K. Lourenssen, J. Williams, F. Ahmadpour, R. Clemmer, and S. Tasnim, "Vanadium redox flow batteries: A comprehensive review," *Journal of Energy Storage*, vol. 25, Oct. 2019, ISSN: 2352152X. DOI: 10.1016/J.EST.2019.100844.

[33] H. T. Do Thi, T. Pasztor, D. Fozer, F. Manenti, and A. J. Toth, "Comparison of Desalination Technologies Using Renewable Energy Sources with Life Cycle, PESTLE, and Multi-Criteria Decision Analyses," *Water 2021, Vol. 13, Page 3023*, vol. 13, no. 21, p. 3023, Oct. 2021, ISSN: 2073-4441. DOI: 10.3390/W13213023. [Online]. Available: https://www.mdpi.com/2073-4441/13/21/3023/htm%20https://www.mdpi.com/2073-4441/13/21/3023.

[34] M. A. Khan, T. Al-Attas, S. Roy, *et al.*, "Seawater electrolysis for hydrogen production: a solution looking for a problem?" *Energy & Environmental Science*, vol. 14, no. 9, pp. 4831–4839, Sep. 2021, ISSN: 1754-5706. DOI: 10.1039/D1EE00870F. [Online]. Available: https://pubs.rsc.org/en/content/articlehtml/2021/ee/d1ee00870f%20https://pubs.rsc.org/en/content/articlelanding/2021/ee/d1ee00870f.

[35] Tennet, "66 kV Systems for Offshore Wind Farms," Tennet, Arnhem, Tech. Rep., 2015.

[36] ITM Power, *ITM Power and Ørsted: Wind Turbine Electrolyser Integration*, 2019.

[37] J. Marchand, A. Shetgaonkar, J. L. R. Torres, A. Lekic, and P. Palensky, "EMT Real-Time Simulation Model of a 2 GW Offshore Renewable Energy Hub Integrating Electrolysers," *Energies*, vol. 14, no. 24, p. 8547, Dec. 2021, ISSN: 1996-1073. DOI: 10.3390/EN14248547. [Online]. Available: https://research.tudelft.nl/en/publications/emt-real-time-simulation-model-of-a-2-gw-offshore-renewable-energ.

[38] H2Dock, *H2Dock - Enabling electrolysis @ sea*. [Online]. Available: https://h2dock.com/.

[39] M. Zaaijer, A. Viré, R. B. Dos, S. Pereira, and A. Daneshbodi, "Introduction to wind turbines: physics and technology Editing (text and videos)," Tech. Rep., 2020.

[40] DNV, "HYDROGEN FORECAST TO 2050," [Online]. Available: https://aben.com.br/wp-content/uploads/2022/06/DNV_Hydrogen_Report_2022_Highres_single1.pdf.

[41] IEA, "The Future of Hydrogen," 2019. [Online]. Available: https://iea.blob.core.windows.net/assets/9e3a3493-b9a6-4b7d-b499-7ca48e357561/The_Future_of_Hydrogen.pdf.

[42] Thyssenkrupp, "Hydrogen from large-scale electrolysis Efficient solutions for sustainable chemicals and energy storage," 2019.

[43] J. Davies, F. Dolci, E. Weidner, and European Commission. Joint Research Centre., "Historical Analysis of FCH 2 JU Electrolyser Projects," ISSN: 1831-9424. DOI: 10.2760/951902. [Online]. Available: https://publications.jrc.ec.europa.eu/repository/handle/JRC121704.

[44] Sunfire, "SUNFIRE-HYLINK ALKALINE FACTSHEET,"

[45] NEL Hydrogen, *Alkaline and Proton PEM Electrolysers | Nel Hydrogen*, 2021. [Online]. Available: https://nelhydrogen.com/resources/electrolysers-brochure/.

[46] Cummins, "WE'RE AT THE HEART OF THE POWER REVOLUTION," 2021.

[47] M. Sánchez, E. Amores, D. Abad, L. Rodríguez, and C. Clemente-Jul, "Aspen Plus model of an alkaline electrolysis system for hydrogen production," *International Journal of Hydrogen Energy*, vol. 45, no. 7, pp. 3916–3929, Feb. 2020, ISSN: 03603199. DOI: 10.1016/J.IJHYDENE.2019.12.027.

[48] R. García-Valverde, N. Espinosa, and A. Urbina, "Simple PEM water electrolyser model and experimental validation," *International Journal of Hydrogen Energy*, vol. 37, no. 2, pp. 1927–1938, Jan. 2012, ISSN: 03603199. DOI: 10.1016/J.IJHYDENE.2011.09.027.

[49] Ø. Ulleberg, "Modeling of advanced alkaline electrolyzers: A system simulation approach," *International Journal of Hydrogen Energy*, vol. 28, no. 1, pp. 21–33, Jan. 2003, ISSN: 03603199. DOI: 10.1016/S0360-3199(02)00033-2.

[50] G. Matute, J. M. Yusta, and L. C. Correas, "Techno-economic modelling of water electrolysers in the range of several MW to provide grid services while generating hydrogen for different applications: A case study in Spain applied to mobility with FCEVs," *International Journal of Hydrogen Energy*, vol. 44, no. 33, pp. 17 431–17 442, Jul. 2019, ISSN: 03603199. DOI: 10.1016/J.IJHYDENE.2019.05.092.

[51] A. K. Shukla, M. K. Ravikumar, and T. S. Balasubramanian, "Nickel/iron batteries," *Journal of Power Sources*, vol. 51, no. 1-2, pp. 29–36, 1994, ISSN: 03787753. DOI: 10.1016/0378-7753(94)01953-3.

[52] CellCube, "Battery technology," 2022.

[53] Invinity, "INVINITY VS3-022 SIX PACK TM VANADIUM FLOW BATTERY," *https://invinity.com/wp-content/uploads/2022/12/Invinity-VS3-022-Vanadium-Flow-Battery-Data-Sheet-MAR00016-2022-11.pdf*, 2022.

[54] T. Wright, "Factors Affecting the Cost of Airplanes," *Journal of the Aeronautical Sciences*, vol. 3, pp. 122–128, 1936. DOI: 10.2514/8.155. [Online]. Available: http://arc.aiaa.org.

[55] I. TSIROPOULOS, D. TARVYDAS, and A. ZUCKER, "Cost development of low carbon energy technologies: Scenario-based cost trajectories to 2050, 2017 edition," *JRC*, 2018, ISSN: 1831-9424. DOI: 10.2760/490059. [Online]. Available: https://publications.jrc.ec.europa.eu/repository/handle/JRC109894.

[56] A. Elia, M. Kamidelivand, F. Rogan, and B. Ó Gallachóir, "Impacts of innovation on renewable energy technology cost reductions," *Renewable and Sustainable Energy Reviews*, vol. 138, Mar. 2021, ISSN: 18790690. DOI: 10.1016/J.RSER.2020.110488.

[57] F. I. Ise, "COST FORECAST FOR LOW TEMPERATURE ELECTROLYSIS-TECHNOLOGY DRIVEN BOTTOM-UP PROGNOSIS FOR PEM AND ALKALINE WATER ELECTROLYSIS SYSTEMS," *https://www.ise.fraunhofer.de/content/dam/ise/de/documents/publications/studies/cost-forecast-for-low-temperature-electrolysis.pdf*, 2021.

[58] Renewable Energy Catapult, "Guide to an offshore wind farm," 2019. [Online]. Available: www.thecrownestate.co.uk.

[59] Renewable Energy Catapult, "FLOATING OFFSHORE WIND CENTRE OF EXCELLENCE," [Online]. Available: https://ore.catapult.org.uk/wp-content/uploads/2021/01/FOW-Cost-Reduction-Pathways-to-Subsidy-Free-report-.pdf.

[60] R. Wiser, J. Rand, J. Seel, *et al.*, "Expert elicitation survey predicts 37% to 49% declines in wind energy costs by 2050," *Nature Energy 2021 6:5*, vol. 6, no. 5, pp. 555–565, Apr. 2021, ISSN: 2058-7546. DOI: 10.1038/s41560-021-00810-z. [Online]. Available: https://www.nature.com/articles/s41560-021-00810-z.

[61] W. Musial, P. Spitsen, P. Duffy, *et al.*, "Offshore Wind Market Report: 2022 Edition," 2022.

[62] R. Williams, F. Zhao, and J. Lee, "Global Offshore Wind Report 2022," *https://gwec.net/wp-content/uploads/2022/06/GWEC-Global-Offshore-Wind-Report-2022.pdf*, 2022. [Online]. Available: www.gwec.net.

[63] McKinsey & Company, *Succeeding in the global offshore wind market | McKinsey*. [Online]. Available: https://www.mckinsey.com/industries/electric-power-and-natural-gas/our-insights/how-to-succeed-in-the-expanding-global-offshore-wind-market.

[64] DNV, "MAINE OFFSHORE WIND ANALYSIS State of the Offshore Wind Industry: Today through 2050 State of Maine Governor's Energy Office," *https://www.maine.gov/energy/sites/maine.gov.en files/Maine%20OSW%20DNV%20Task%201%20-%20State%20of%20the%20OSW%20Industry_Final.p* 2022. [Online]. Available: www.dnv.com.

[65] DNV, "The rise of renewables - DNV," Tech. Rep., 2022. [Online]. Available: https://www.dnv.com/energy-transition-outlook/rise-of-renewables.html.

[66] IEA, *Electrolysers – Analysis - IEA*. [Online]. Available: https://www.iea.org/reports/electrolysers.

[67] I. Renewable Energy Agency, "GLOBAL HYDROGEN TRADE TO MEET THE 1.5°C CLIMATE GOAL PART I TRADE OUTLOOK FOR 2050 AND WAY FORWARD," 2022. [Online]. Available: www.irena.org/publications.

[68] Hydrogen Counsil, "Path to hydrogen competitiveness A cost perspective," 2020. [Online]. Available: www.hydrogencouncil.com..

[69] M. Junginger and A. Louwen, "Technological learning in the transition to a low-carbon energy system: Conceptual issues, empirical findings, and use in energy modeling," *Technological Learning in the Transition to a Low-Carbon Energy System: Conceptual Issues, Empirical Findings, and Use, in Energy Modeling*, pp. 321–326, Jan. 2019. DOI: 10.1016/C2018-0-04547-8.

[70] M. Barnard, *Agora CO2 Redox Battery Wins Global Deeptech Competitions & Has 1 Year ROI - CleanTechnica*, 2021. [Online]. Available: https://cleantechnica.com/2021/08/14/agora-co2-redox-battery-wins-global-deeptech-competitions-has-1-year-roi/.

[71] McKinsey, *The clean hydrogen opportunity | McKinsey*, 2022. [Online]. Available: https://www.mckinsey.com/industries/oil-and-gas/our-insights/the-clean-hydrogen-opportunity-for-hydrocarbon-rich-countries.

[72] CellCube, "TECHNICAL SPECIFICATION CellCube FB 500-2000 CellCube FB 250-1000 CellCube FB 250-2000," [Online]. Available: www.cellcube.com.

A

Appendix

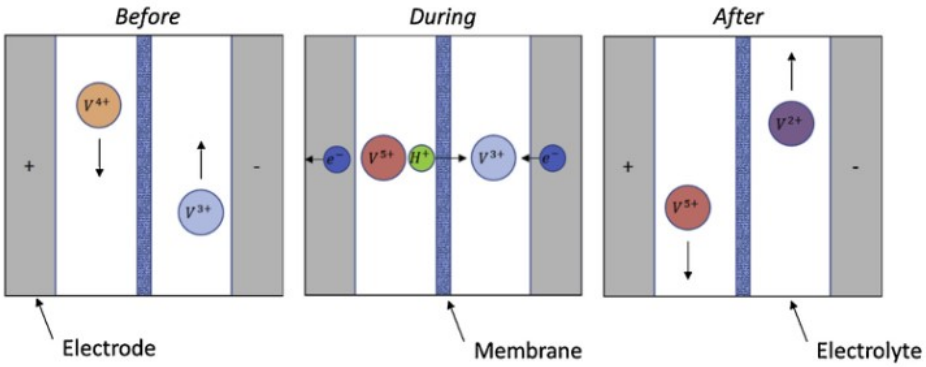

Figure A.1: Schematic representation of the charging process of a vanadium redox flow battery [32]

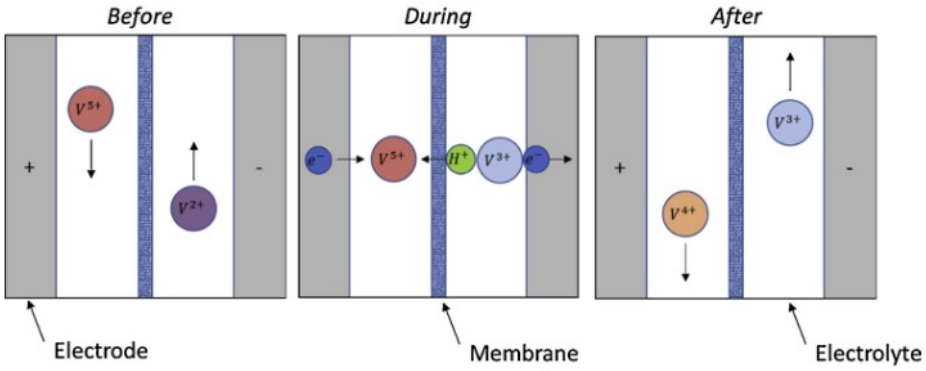

Figure A.2: Schematic representation of the discharging process of a vanadium redox flow battery [32]

B

B

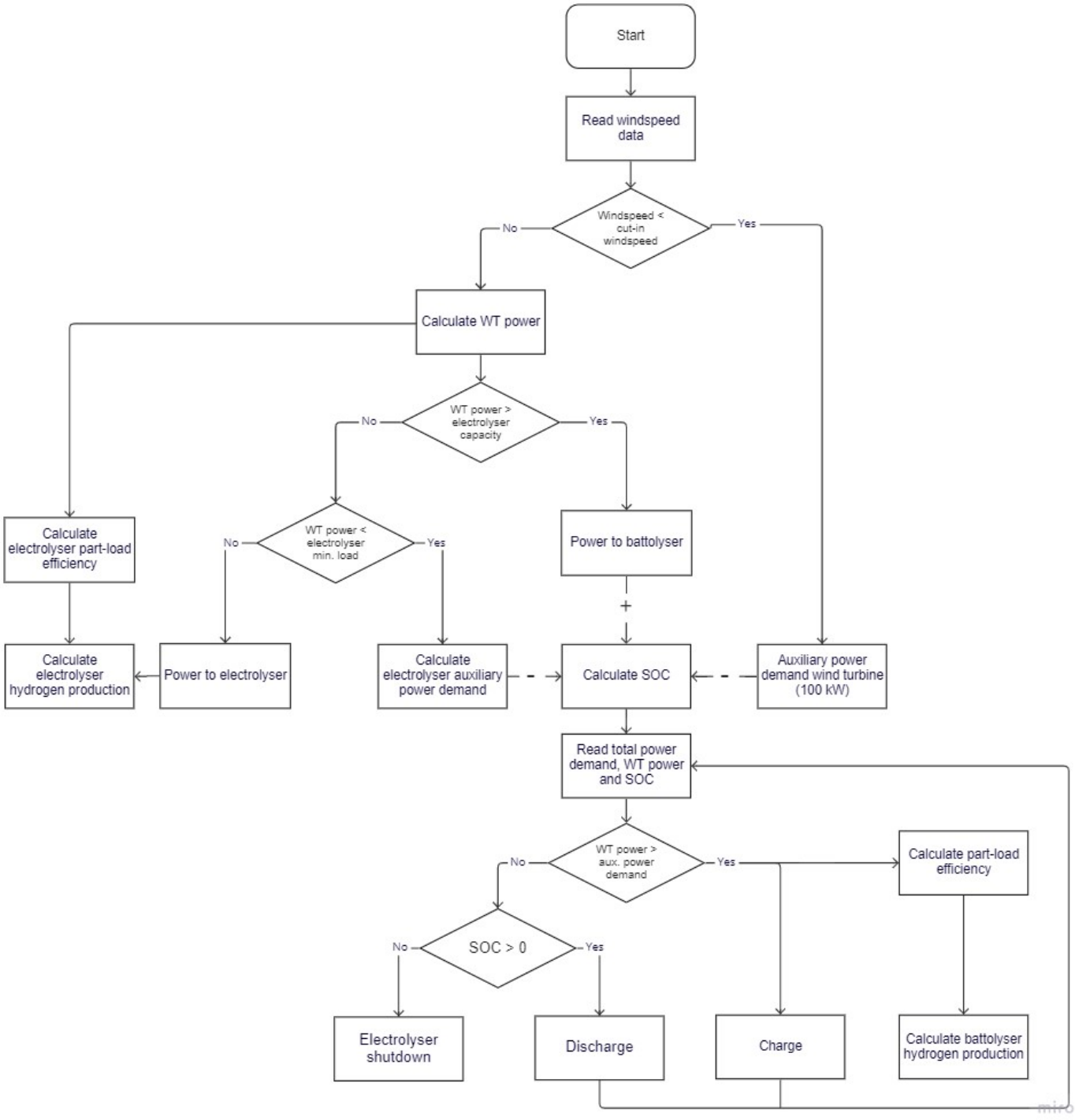

Figure B.1: Schematic representation of the charging process of a vanadium redox flow battery [32]

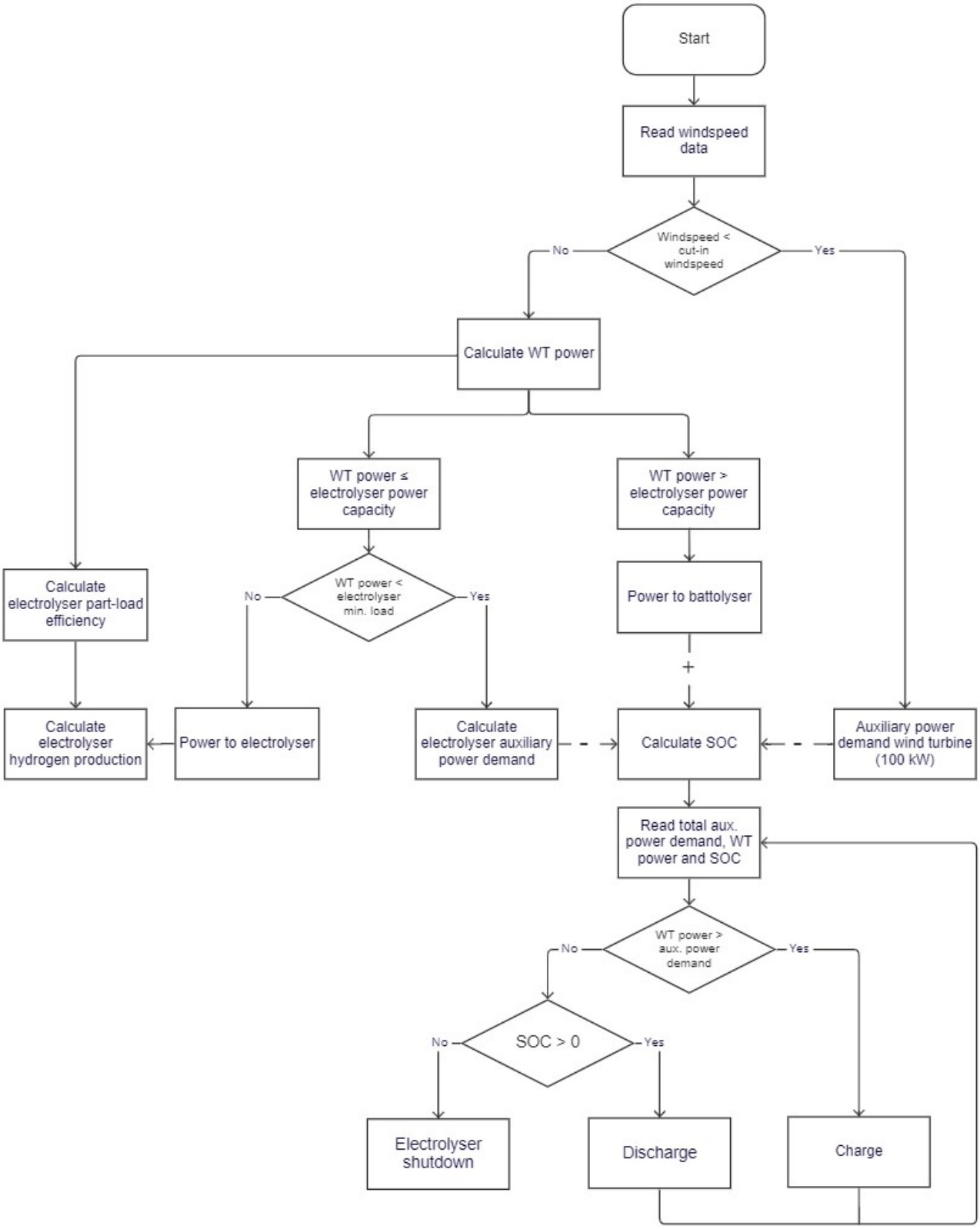

Figure B.2: Schematic representation of the charging process of a vanadium redox flow battery [32]

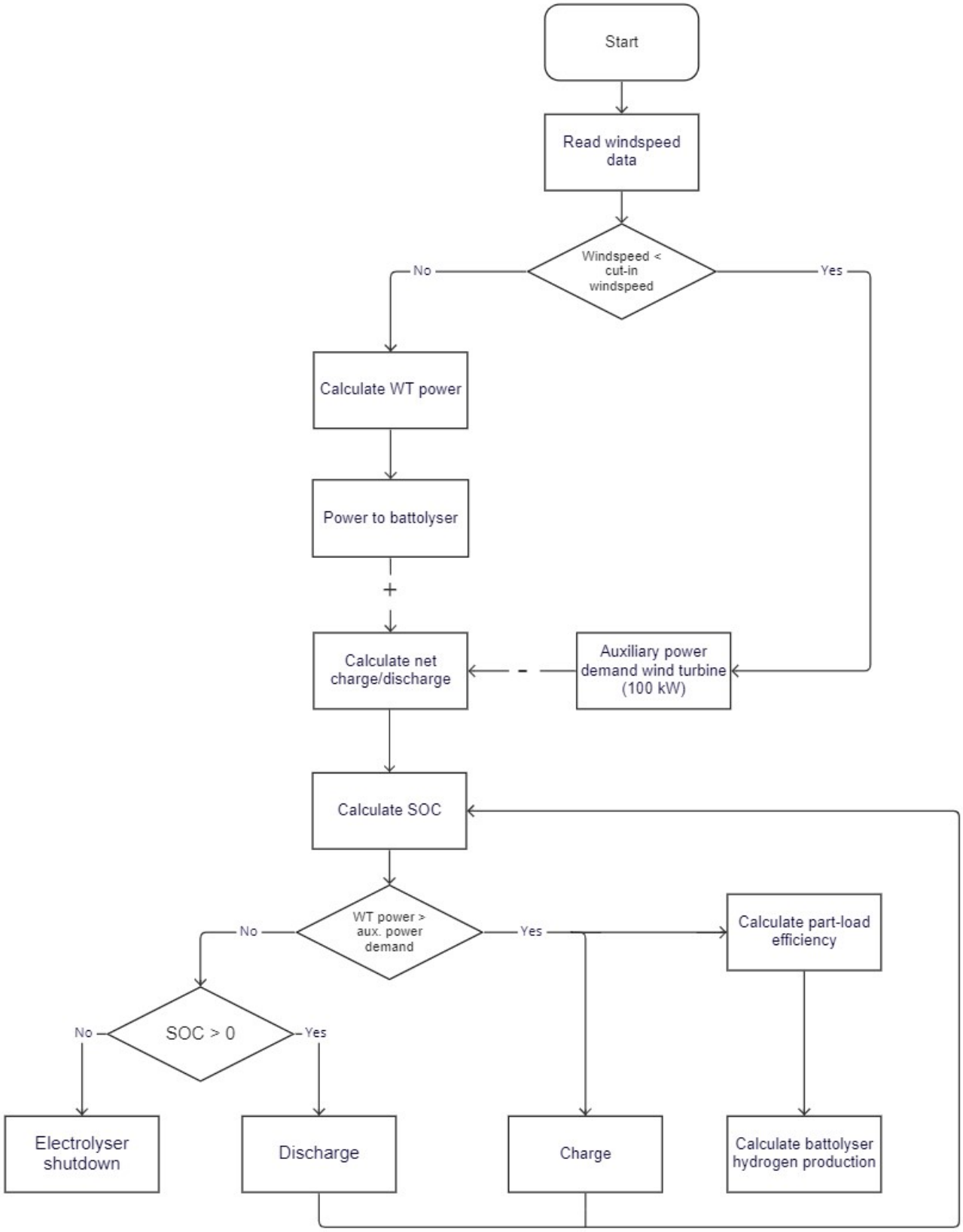

Figure B.3: Schematic representation of the charging process of a vanadium redox flow battery [32]

Catapult data	Rounded cost (£/MW)	(€/MW)
Development and project management	**120000**	**140400**
Development and consenting services	50000	58500
Environmental surveys	4000	4680
Resource and metocean assessment	4000	4680
Geological and hydrological surveys	4000	4680
Engineering and consultancy	4000	4680
Other	54000	63180
Turbine	**1000000**	**1170000**
Nacelle	400000	468000
Rotor	190000	222300
Tower	70000	81900
Other	340000	397800
Balance of plant	**603000**	**331110**
Cables	170000	
Turbine foundation	280000	327600
Offshore substation	120000	
Onshore substation	30000	
Operations base	3000	3510
Installation and commissioning	**650500**	**427635**
Foundation installation	100000	117000
Offshore substation installation	35000	
Onshore substation construction	25000	
Onshore export cable installation	5000	
Offshore cable installation	220000	
Turbine installation	50000	58500
Offshore logistics	3500	4095
Other	212000	248040
Operation, maintenance and servive (per annum)	**75000**	**67860**
Operations	25000	29250
Maintenance and service	50000	38610
Decommissioning	**325000**	**140400**
Turbine decommissioning	45000	52650
Foundation decommissioning	75000	87750
Cable decommissioning	140000	
Substation decommissioning	65000	
Total	**2481213**	**2169718**
Total OPEX	75000	67860
Total CAPEX	2406213	2101858

Figure B.4: Cost breakdown of a 1 GW offshore wind farm [58]

EUR/kW$_{AC}$	PEM Electrolysis				Alkaline Electrolysis			
Year	**2020**		**2030**		**2020**		**2030**	
Capacity (MW$_{AC}$)	**5**	**100**	**5**	**100**	**5**	**100**	**5**	**100**
Electrolysis Stacks	294	212	205	143	185	149	99	64
Power electronics	195	193	123	122	160	159	102	101
High Voltage Transformer	0	25	0	27	0	25	0	26
BoP Cathode + H_2 Purification	76	18	82	18	80	22	83	21
BoP Anode	26	18	25	12	24	16	24	12
H_2O Purification	9	1	10	1	9	1	9	1
System Cooling	12	6	10	5	10	4	9	4
Compression	0	0	0	0	123	47	128	49
Piping	98	90	73	63	95	88	70	60
Instrumentation	122	71	91	49	118	70	88	48
Housing	19	19	15	15	22	22	19	19
Engineering	128	65	95	46	124	60	95	40
SUMME	**978**	**718**	**729**	**502**	**949**	**663**	**726**	**444**

Figure B.5: Cost breakdown of an alkaline and PEM electrolyser in for the years 2020 and 2030 [57]